

Massive Dark Matter Halos around Bright Isolated Galaxies in the 2dFGRS

Peder Norberg^{1,2,3}, Carlos S. Frenk¹ & Shaun Cole¹

¹*Institute for Computational Cosmology, Department of Physics, University of Durham, South Road, Durham DH1 3LE, UK.*

²*ETHZ Institut für Astronomie, HPF G3.1, ETH Hönggerberg, CH-8093 Zürich, Switzerland.*

³*SUPA*, Institute for Astronomy, University of Edinburgh, Royal Observatory, Blackford Hill, Edinburgh, EH9 3HJ, UK.*

28 October 2018

ABSTRACT

We identify a large sample of isolated bright galaxies and their fainter satellites in the 2dF Galaxy Redshift Survey (2dFGRS). We analyse the dynamics of ensembles of these galaxies selected according to luminosity and morphological type by stacking the positions of their satellites and estimating the velocity dispersion of the combined set. We test our methodology using realistic mock catalogues constructed from cosmological simulations. The method returns an unbiased estimate of the velocity dispersion provided that the isolation criterion is strict enough to avoid contamination and that the scatter in halo mass at fixed primary luminosity is small. Using a maximum likelihood estimator that accounts for interlopers, we determine the satellite velocity dispersion within a projected radius of $175 h^{-1}$ kpc. The dispersion increases with the luminosity of the primary and is larger for elliptical galaxies than for spiral galaxies of similar b_J luminosity. Calibrating the mass-velocity dispersion relation using our mock catalogues, we find a dynamical mass within $175 h^{-1}$ kpc of $M_{175}/h^{-1}M_{\odot} \simeq 4.0_{-1.5}^{+2.3} \times 10^{12} (L_{b_J}/L_*)$ for elliptical galaxies and $M_{175}/h^{-1}M_{\odot} \simeq 6.3_{-3.1}^{+6.3} \times 10^{11} (L_{b_J}/L_*)^{1.6}$ for spiral galaxies. Finally, we compare our results with recent studies and investigate their limitations using our mock catalogues.

Key words: galaxies: halos - galaxies: kinematics & dynamics - galaxies: mass - galaxies: satellites - galaxies: spiral - surveys

1 INTRODUCTION

The view that galaxies are surrounded by large dark matter halos dates back more than 30 years to the pioneering study of the rotation curve of M32 by Rubin & Ford (1970). Extended galactic halos are, in fact, a generic feature of the cold dark matter model of galaxy formation (Blumenthal et al 1984, Frenk et al 1985), but this fundamental theoretical prediction has limited observational support. Zaritsky et al. (1993) attempted to measure the mass and extent of dark matter halos by analysing the dynamics of satellite galaxies found around ‘isolated’ galaxies. Since galaxies generally have only a few detectable satellites, they used a method that consists of stacking satellites in a sample of primaries of similar luminosity. In spite of the small size of their relatively inhomogeneous sample, Zaritsky et al. (1993) were able to detect massive halos around isolated spiral galaxies extending to many optical radii. Having nearly doubled their satellite sample to 115 members, Zaritsky et al. (1997b) confirmed their earlier claims including a puzzling lack of correlation between the velocity dispersion of the (stacked) satellite system and the luminosity of the primary.

More recently, McKay et al. (2002) performed a similar

analysis on data from the Sloan Digital Sky Survey (SDSS; York et al. 2000). They compared mass estimates derived from satellite dynamics to those derived from weak lensing analyses of the same data (McKay et al. 2001). With a much larger sample than that of Zaritsky et al (1997), they were able to detect a correlation between satellite velocity dispersion and primary luminosity. This trend was confirmed by Prada et al. (2003) who also used SDSS data. Although they are both based on SDSS data, these two studies find results that, while consistent at first sight, are in, fact, somewhat contradictory. For example, although Prada et al (2003) found a strong dependence of satellite velocity dispersion on galactocentric distance, their measured velocity dispersion within a radius of $125 h^{-1}$ kpc is similar to the values obtained by McKay et al. (2002) at a radius of $275 h^{-1}$ kpc. Discrepant results were also found by Brainerd & Specian (2003) who applied the same technique to the early, “100k” data release of the 2degree-Field Galaxy Redshift Survey (2dFGRS; Colless 2001) and derived satellite velocity dispersions which are in qualitative and quantitative disagreement with those of Zaritsky et al. (1997), McKay et al. (2002) and Prada et al. (2003). A more extensive analysis of the complete 2dFGRS (Colless et al. 2003) by Brainerd (2005) also led to disagreements with the results of earlier work. This somewhat confused picture of

* The Scottish Universities Physics Alliance

satellite dynamics is due in large part to different choices of primary galaxy samples and to differences in the modelling and analysis methods.

This paper has multiple aims. Firstly, we carry out a new analysis of the dynamics of satellites around bright galaxies of different morphological types selected from the full 2dFGRS. The goal is to constrain the velocity dispersion and mass of their dark matter halos and we therefore select a sample of isolated galaxies chosen according to strict criteria. Secondly, we investigate the reliability and accuracy of commonly used dynamical analysis methods. For this, we make extensive use of realistic mock catalogues constructed from large cosmological N-body simulations and different semi-analytic galaxy formation models (Cole et al. 2000; Springel et al. 2001). A similar approach, but in a different context, was adopted by van den Bosch et al. (2004). Finally, we attempt to understand the root cause of the differences found in previous work, again relying on the use of realistic mock catalogues.

The paper is organised as follows. In Section 2, we briefly present some of the characteristics of the 2dFGRS data and simulations used for our analysis. In Section 3, we describe the satellite sample selection scheme, together with its robustness to changes in the selection parameters. The analysis of the 'stacked' satellite velocity distribution is carried in Section 4 while, in Section 5, we present velocity dispersion estimates for our mock catalogues and for 2dFGRS primaries split according to luminosity and morphological type. Using a model for the relationship between dark halo mass and satellite velocity dispersion, we give, in Section 6, an estimate of the mass of the halos around 2dFGRS galaxies. In Section 7, we compare our results with those of previous studies, and we conclude in Section 8.

2 THE DATA

2.1 The 2dFGRS data

Detailed descriptions of the construction of the 2dF Galaxy Redshift Survey (2dFGRS) and its properties are given in Colless et al. (2001; 2003). In summary, galaxies are selected down to a magnitude limit of $b_J \approx 19.45$ from the full 2dFGRS catalogue, with $\sim 225\,000$ galaxies having a "good quality" redshift measurement. We restrict our analysis to the two large contiguous volumes of the survey, one centred on the Southern Galactic Pole (SGP) and the other close to the direction of the Northern Galactic Pole (NGP).

Three limitations of the 2dFGRS catalogue are relevant for this work. Firstly, the 2dFGRS source catalogue, based on the APM galaxy catalogue, is not complete. By comparing the 2dFGRS with the SDSS, Norberg et al. (2002) estimated the completeness of the 2dFGRS to be $\sim 91\% \pm 2\%$, and ascribed the incompleteness primarily to misclassification of APM images. Misclassification of close galaxy pairs will cause some true pairs to be missed from our sample of primaries. The 2dFGRS suffers from an additional form of close pair incompleteness due to 'fibre collisions' during the spectroscopic observations. The observing strategy employed in the 2dFGRS, consisting of a set of overlapping tiles which are successively observed, was designed to minimise the number of 'fibre collisions', and the remaining incompleteness is very precisely quantified (Colless et al. 2001).

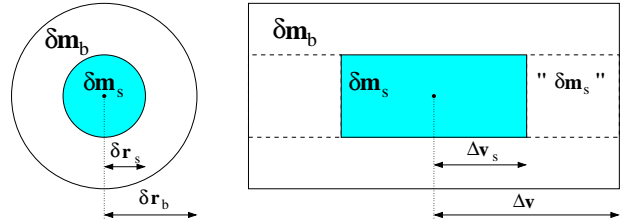


Figure 1. A schematic of the isolation criterion. The figure on the left shows the projection on the sky of the cylinder that defines the primary isolation criterion. The figure on the right shows the configuration as seen along the redshift axis. The central point in each panel corresponds to a primary; only galaxies located in the shaded area are considered as potential satellites.

Finally, the *rms* accuracy of redshift measurements for a typical galaxy is 85 km s^{-1} and tends to be slightly larger for the faintest galaxies and slightly smaller for the brighter ones (Colless et al. 2001).

Since we are primarily interested in the velocity dispersion at large radius, the close pair incompleteness in the catalogue does not have an important effect on our conclusions. Nevertheless, it is important to model carefully both the incompleteness and the velocity errors and to include these in the construction of our mock galaxy catalogues.

Finally, we make use of the 'eyeball' morphological classification carried out by Loveday et al. (1996) based on the APM images. This is available for 80% of the central galaxies in our sample. We prefer this classification to the more objective spectral classification of Madgwick et al. (2002) because aperture effects are important for our sample of relatively nearby galaxies. However, we have repeated the analysis of section 5.2 using subsamples defined by their spectral classification and find no difference in our results within the errors.

2.2 The Λ CDM Simulation

We use mock 2dFGRS catalogues constructed from cosmological simulations in order to assess the extent to which the various limitations of the data affect our results. In particular, we use the mocks to investigate possible systematic effects arising from our method for selecting satellites, as well as from our procedure of stacking satellites together. The mock catalogues allow us also to investigate the effects of redshift space distortions and redshift measurement errors. In the simulations we, of course, know not only the redshifts of galaxies but also their distances. In what follows, we use the term "real space" to refer to measurements that make use of the true 3-d position and the term "redshift space" to refer to measurements that make use of pseudo 3-d positions, i.e. those for which the distance to the galaxy is given by the sum of the pure Hubble flow distance and the peculiar velocity along the line-of-sight, in units of $h^{-1} \text{Mpc}$.

To construct mock 2dFGRS catalogues, we use a high-resolution N-body simulation of a flat, Λ -dominated cold dark matter universe with the following parameters: matter density, $\Omega_m = 0.3$; cosmological constant term, $\Omega_\Lambda = 0.7$; Hubble constant, $H_0 = 70 \text{ km s}^{-1} \text{Mpc}^{-1}$; index of primordial fluctuation power spectrum, $n = 1$; and present-day

Table 1. Properties of the combined NGP & SGP satellite samples around bright galaxies, for different values of N_{viol} and for different primary morphological type. The numbers quoted in brackets are after small groups are excluded from the full satellite sample. r_p is in h^{-1} kpc.

Sample	Primary Type	N_{viol}	N_{prim}	N_{sat}	$N_{\text{sat}}(r_{\text{int}} < r < r_{\text{ext}})$		
					$0 < r_p < 175$	$40 < r_p < 175$	$40 < r_p < 175$
2dFGRS	any	0	362 (357)	642 (588)	273	241	
2dFGRS	any	4	571 (564)	1003 (918)	434	383	
2dFGRS	Spiral-Irregular	0	203 (203)	322 (322)	141	120	
2dFGRS	Spiral-Irregular	4	311 (311)	465 (465)	210	181	
2dFGRS	Elliptical-S0	0	85 (81)	203 (161)	75	69	
2dFGRS	Elliptical-S0	4	141 (135)	338 (265)	118	111	
Mock	any	0	387 (387)	648 (648)	384	231	
Mock	any	4	736 (736)	1226 (1226)	723	442	

fluctuation amplitude $\sigma_8 = 0.9$. The simulation followed 400^3 particles in a box of side $110 h^{-1}$ Mpc (see Gao et al. (2004) for a full description of the simulation). The simulation was populated with galaxies by applying the ‘‘Munich’’ semi-analytic model of galaxy formation to the merger trees of each halo (Springel et al. 2001). In this model, galaxies reside in resolved halos and their subhalos. When a subhalo is no longer resolved, the galaxy is placed on the most bound particle of the subhalo when it was last resolved and an analytic dynamical friction calculation is used to determine when a satellite merges with the central galaxy. The free parameters of the model are tuned to match the Tully-Fisher relation, the B-band cluster galaxy luminosity function and the overall two-point correlation function (Springel et al. 2001). An interesting feature of this semi-analytic galaxy formation model is the generation of a velocity bias between galaxies and dark matter, as function of halo radius.

In order to obtain as close a match as possible between the 2dFGRS selection function and that in the mocks, we rescale the luminosities of the model galaxies preserving the luminosity ranking so that their luminosity function exactly matches that of the 2dFGRS (Norberg et al. 2002). The required rescaling can be as large as a magnitude for some of the mock galaxies, but the differential rescaling for galaxies brighter than $M_{\text{b},j} - 5\log_{10}h < -18$, which make up the bulk of our sample of primaries, is small. Thus, for these brighter galaxies, the magnitude differences are quite accurately preserved. We then extract magnitude-limited catalogues of galaxies to the same magnitude limit and with the same geometry as the real 2dFGRS, as described by Norberg et al. (2002). This requires using three periodic replications of the simulation cube. (We have checked that removing any duplicated systems does not affect any of our results.)

The last step is to create ‘sampled’ mocks by applying the 2dFGRS masks (including the redshift incompleteness mask) and the 2dFGRS photometric errors, as explained in greater detail in Norberg et al. (2002). Finally, we add to each observed velocity an ‘‘observational error’’ randomly sampled from a Gaussian of width 80 km s^{-1} . This value is a compromise between the Gaussian errors measured from repeat observations for our sample of 2dFGRS primaries ($\sigma \simeq 70 \pm 7 \text{ km s}^{-1}$) and satellites ($\sigma \simeq 86 \pm 5 \text{ km s}^{-1}$).

3 SATELLITE SAMPLE

We begin this section by explaining the method used to define the satellite sample, which is applied to both the 2dFGRS data and the mock catalogues. We then briefly consider the robustness of the satellite properties to variations of the selection parameters, an issue that we address further in the appendices. Finally, we present some general properties of the satellite samples used in this paper.

3.1 Satellites around Isolated Primaries

Since the main purpose of our analysis is to constrain the mass of the galactic halo using the dynamics of satellites, we require a sample of isolated primaries. To construct it, we begin by excluding regions in the 2dFGRS that could be contaminated by large clusters. Specifically, we exclude regions lying within three projected Abell radii ($3 \times 1.5 h^{-1}$ kpc) and 3000 km s^{-1} of the centre of clusters in the catalogue of Dalton et al. (1997). Next, we select a sample of bright, isolated primaries by requiring that they satisfy the following criteria:

- the local 2dFGRS magnitude limit should be at least $\delta m_s = 2.2$ fainter than the primary
- all the neighbouring galaxies within $\Delta V = |V^{\text{prim}} - V^{\text{gal}}| \leq 2400 \text{ km s}^{-1}$ and within a projected radius $\delta r_s \leq 400 h^{-1}$ kpc should be faint enough to satisfy $b_j^{\text{gal}} - b_j^{\text{prim}} \geq \delta m_s = 2.2$
- all neighbouring galaxies within $\Delta V = |V^{\text{prim}} - V^{\text{gal}}| \leq 2400 \text{ km s}^{-1}$ and within a projected radius $\delta r_b \leq 1000 h^{-1}$ kpc should satisfy $b_j^{\text{gal}} - b_j^{\text{prim}} \geq \delta m_b = 0.8$,

where the projected radius between two galaxies, at positions \mathbf{r}_1 and \mathbf{r}_2 , is defined by:

$$\delta d = 2 \frac{|\mathbf{r}_1 + \mathbf{r}_2|}{2} \sqrt{\frac{1 - \cos(\alpha)}{1 + \cos(\alpha)}} \quad \text{with } \cos(\alpha) = \frac{\mathbf{r}_1 \cdot \mathbf{r}_2}{|\mathbf{r}_1| |\mathbf{r}_2|}. \quad (1)$$

All galaxies that lie within a projected distance $\leq 400 h^{-1}$ kpc of a primary and have relative velocity $\Delta V_s = |V^{\text{prim}} - V^{\text{gal}}| \leq 1200 \text{ km s}^{-1}$ are considered as potential satellites. The isolation criterion is presented in schematic form in Fig. 1.

Our adopted value of δm_s corresponds to a factor of 8 in luminosity and a similar factor in mass. The primary motivation behind this choice is to ensure that the satellites are small enough to produce only minor perturbations in the gravitational potential of the system. As shown in section 5,

our galaxy mock catalogues indicate that our adopted value is adequate. A more detailed discussion of the precise choice of δm_s may be found in Appendix A.

Since not all galaxies in the 2dFGRS have a measured redshift, the primary isolation criterion could be violated by galaxies that lack a redshift measurement. We can guard against this by eliminating all primaries that could have their isolation criterion violated by such galaxies. A less restrictive condition is to accept only those for which it could be violated by at most N_{viol} galaxies. A conservative estimate of N_{viol} follows from taking all galaxies without redshift to be at the redshift of the primary and checking whether this would cause the primary to violate the isolation criterion. In what follows, we adopt a value of $N_{\text{viol}} = 4$. We have checked that none of our results are influenced by the precise choice of N_{viol} used. The only effect of adopting $N_{\text{viol}} = 4$, rather than $N_{\text{viol}} = 0$, is to increase the number of satellites and hence the signal-to-noise of our measurements. With this choice of N_{viol} , the satellite sample is $\sim 55\%$ larger than for $N_{\text{viol}} = 0$ ($\sim 45\%$ for spirals and $\sim 65\%$ larger for ellipticals). The largest increase occurs for the faintest absolute magnitude bins for which the number of satellites nearly doubles.

With this algorithm and using the values of the selection parameters specified above, we identify 571 primary galaxies surrounded by 1003 satellites. The algorithm also detects over 1500 isolated galaxies without spectroscopically confirmed satellites brighter than the local magnitude limit, but these have over 2200 neighbours without measured redshift which could in principle be satellites. Some of these statistics are summarised in Table 1.

Applying the same selection criterion to the mock catalogues, we identify, in real space, 750 primary galaxies surrounded by 1241 satellites. In real space, the isolation criterion is slightly different: instead of two cylinders of length ΔV and ΔV_s , we use two spheres of radius δr_b and δr_s respectively. The requirements on the magnitude differences remain the same. All galaxies within δr_s of the primary are considered as satellites. In redshift space, including velocity errors, we find 736 primary galaxies surrounded by 1226 satellites. As for the real data, the algorithm detects a further 1500 primaries without any confirmed satellite, but with 1700 possible candidates without measured redshifts.

3.2 Robustness of the satellite detection algorithm

It is important to test the dependency of the satellite detection algorithm on the values of the selection parameters. We find that the size of the satellite sample and its properties are not very sensitive to the specific values of the inner and outer projected radii, so long as the exclusion criterion does not become too restrictive. The adopted values for these parameters represent a compromise between having a dynamically isolated system and a large sample of satellites.

On the other hand, the inner and outer cylinder depths have a non-trivial influence on the satellite sample. First, if the ‘velocity difference’ between ΔV_s and ΔV is less than ΔV_s^1 , then there is the potential risk of finding a single satel-

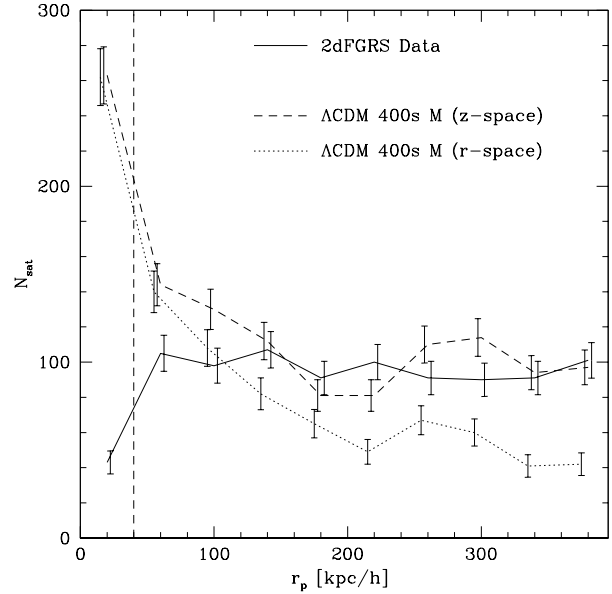


Figure 2. Transverse distributions of satellites: comparison between satellite samples extracted from the 2dFGRS (solid bold line), from the mocks in redshift space (dashed line) and in real space (dotted line). The vertical dashed line indicates the limiting projected radii, as used for the ‘ r_p cut’ (see text). The errorbars plotted assume Poisson statistics.

lite galaxy associated with two different primaries. In such a case, neither primary can be considered isolated. Therefore in order to avoid this problem and obtain a self consistent isolation criterion, we always impose $|\Delta V - \Delta V_s| \geq \Delta V_s$. We note that none of the previous work in this subject has included such a constraint. It is not clear if their samples had any shared satellites and if they did how they were treated, but we note that for both the 2dFGRS data and our mock galaxy catalogues, this subtle problem does occur.

Secondly, if the outer depth of the cylinder, i.e. ΔV , is very large, the isolation criterion is more stringent, and our catalogue will contain fewer primaries. Conversely if ΔV is too small the isolation criterion becomes too relaxed and we risk including non-isolated systems in our sample.

Finally, if ΔV_s increases the contamination of the satellite sample by interlopers² is increased. For instance, when increasing ΔV_s from 600 km s^{-1} to 1800 km s^{-1} , we see a flattening of the velocity distribution, which we interpret as being due to interlopers in our satellite catalogue. Conversely too small a value of ΔV_s would mean that the full width of the velocity distribution that we are trying to characterise would not be sampled. It is essential that ΔV_s be greater than 3 to 4 σ , where σ is rms width of the underlying satellite velocity distribution.

Therefore the choice of $\Delta V = 2400 \text{ km s}^{-1}$ and $\Delta V_s =$

¹ i.e. $|\Delta V - \Delta V_s| \leq \Delta V_s$

² In the mock catalogues we can label any galaxy that is selected as a satellite, but does not reside within the dark matter halo of the primary galaxy as an interloper. In the real data this is not possible, but one can still statistically estimate the fraction of interlopers by their effect on the satellite velocity distribution (see section 4.2).

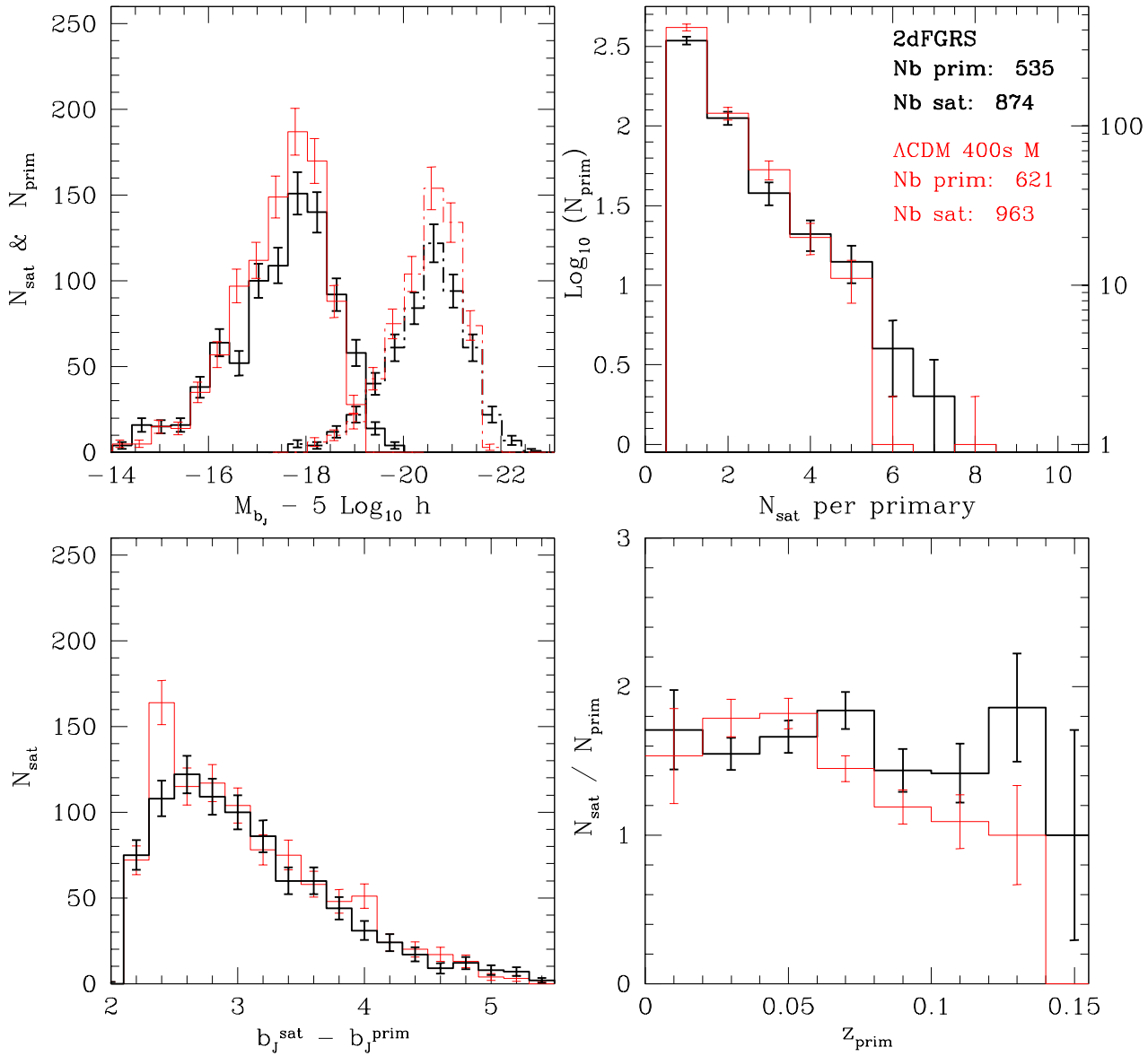


Figure 3. Statistics of primary galaxies and their associated satellites: in all panels we adopt a thick line style for 2dFGRS data and a thin line style for final mock data. All errorbars assume Poisson statistics. The top left panel shows the distribution of absolute magnitudes of satellites (solid line) and primaries (dot-dashed line). The top right panel shows the distribution of the number of satellites per primary. The bottom left panel shows the distribution of the magnitude difference between primary and satellite. The bottom right panel shows the fraction of satellites per primary as function of redshift. All panels are done using the satellite samples obtained by applying the isolation criterion, rejecting small groups and with ‘ r_p cut’. See text for more details.

1200 km s⁻¹ is a compromise between reducing the catalogue contamination from interlopers, increasing the size of the satellite catalogue and allowing a robust velocity dispersion estimate to be obtained. We note that the choice of the depth of the cylinders could be tuned with the size of the system considered to increase the efficiency with which ‘small’ systems are detected. This is a point to which we return in section 5.

In the appendices, we discuss in detail the isolation cri-

teria proposed by McKay et al. (2002), Prada et al. (2003), Brainerd & Specian (2003), van den Bosch et al. (2004) and Brainerd (2005). The summary of those findings is given in section 7.

3.3 General Properties of Satellite Samples

Before performing a detailed dynamical study, we focus briefly on some general properties of the satellite samples.

This leads us to make some additional cuts to improve the match between observed and mock samples.

3.3.1 Transverse distributions of satellites

In Fig. 2, we present the distribution of transverse separations for three satellite samples. The mock satellite samples selected both in real and redshift space have centrally peaked distributions with the redshift space selected sample having the flatter distribution at separations $r_p > 100 h^{-1}$ kpc. In contrast the data has a almost flat distribution throughout $100 < r_p < 350 h^{-1}$ kpc, but with a significant drop in the central region. The reasons behind this difference on small scales are multiple: first of all, the 2dFGRS input catalogue lacks close galaxy pairs (Norberg et al. 2002) and this deficit is enhanced by the targets that are rejected due to fibre collisions; secondly galaxies are not point source objects, but extended objects on the sky, which means that the innermost radial bin can suffer from projection effects which are not taken into account in the mocks (see van den Bosch et al. (2005) for a more detailed study of this particular issue). Finally, the large number of satellites in the innermost radial bin is not a generic model prediction: their number is sensitive to details of the dynamical friction prescription used in the semi-analytic model.

We could model this limitation in the mock catalogues, by e.g. implementing a supplementary incompleteness around each primary. However, we preferred not to add an arbitrary incompleteness model to our analysis, and hence choose to restrict some comparisons to satellite samples with satellites $r_p > 40 h^{-1}$ kpc. Hereafter we refer to this as the ‘ r_p cut’. The vertical line in Fig. 2 indicates this inner limiting projected radius. Beyond this radius, the distributions of transverse separations for satellites from the mocks (in redshift space) and from the 2dFGRS are in approximate agreement.

3.3.2 Satellite sample properties

In Fig. 3, we present general properties from the mock and data satellite samples (with light and bold line-styles respectively). The data and the semi-analytic mock satellite samples have very similar properties: the peak of the satellite and primary absolute magnitude distributions are roughly the same for both samples, with primaries being typically one magnitude brighter than M^* (top left panel of Fig. 3); the fraction of satellites per primary does not vary significantly as function of redshift; the overall distribution of satellite-primary magnitude differences is similar for both samples, as is the shape of the distribution of the number of satellites per primary (top right panel of Fig. 3).

The good match between data and mock satellite samples, shown in Fig. 3, is achieved after applying both the ‘ r_p cut’ and an additional cut to remove small groups from the 2dFGRS sample. We have removed all primaries which have 9 or more satellites. In the mock catalogue there is only one primary with more than 6 satellites, but in the 2dFGRS there are a few primaries, satisfying the isolation criterion, with 9 or more satellites. Most of them, more than 85%, have primaries that are elliptical galaxies. Removing these systems reduces our 2dFGRS satellite sample by 85 satellites

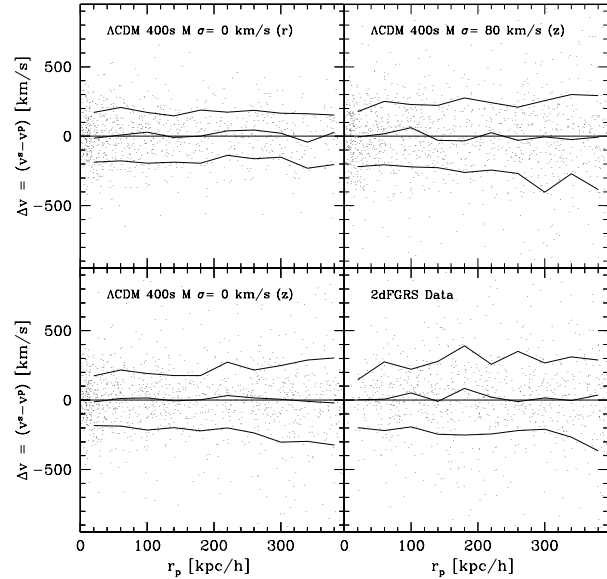


Figure 4. Velocity difference of satellite galaxies and primaries versus transverse separation for the 2dFGRS sample (bottom right panel) and for the mock samples: real space (top left panel); redshift space without velocity errors (bottom left panel) and with velocity errors (top right panel). The solid lines show respectively the 16th, 50th and 84th percentiles of the distribution, in bins of $40 h^{-1}$ kpc. This plot has not been corrected for interlopers.

and reduces the the average number of satellites per primary from ~ 1.75 to ~ 1.63 . The reason for removing them is to both achieve a better match between the mock and 2dFGRS samples and to avoid our dynamical estimates being dominated by these small groups. We could have achieved this second goal by retaining the groups, but down weighting them by giving equal weight per primary rather than per satellite. However, we find that within the errors this does not change our results.

In summary, with these extra restrictions, we end up with mock satellite samples which are rather similar to the 2dFGRS satellite samples.

4 MODELLING THE SATELLITE VELOCITY DISPERSION

In this section, we consider the dynamical properties of the satellite samples obtained in section 3. We start by looking at the satellite velocity distributions, then address the issue of interlopers and background subtraction. Once they are well understood, we devise a method to estimate the satellite velocity dispersion of stacked primaries.

4.1 Velocity Distribution of Satellites

Fig. 4 is a scatter plot showing, for the 2dFGRS data and the mock samples, the satellite galaxy velocity difference (with respect to its associated primary) versus its projected distance from the primary. In all panels, the velocity distribution is rather symmetric around zero for all projected distances. The precise choice of the cylinder depth (as fixed

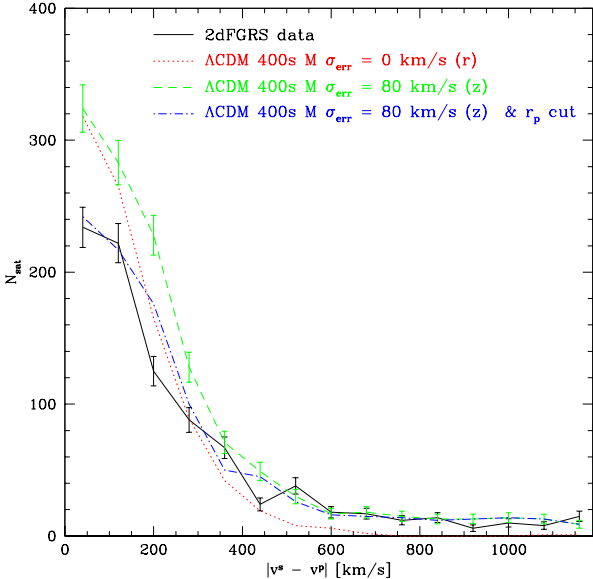


Figure 5. Velocity distributions of satellites within a projected radius of $400 h^{-1}$ kpc: comparison between 2dFGRS satellite sample (solid bold line) and the mock samples in real and redshift space (with and without ‘ r_p cut’). Errorbars, only plotted on two of the curves for visibility, assume Poisson statistics. See text for discussion.

by ΔV and ΔV_s) does not have a strong influence on the distribution for either data or mock, except that the 16th and 84th percentiles become slightly more noisy as the sample size is reduced. There is no strong correlation between velocity difference of the satellite-primary pair and the satellite’s projected distance from the primary. We note that Fig. 4 has not been corrected for interlopers, an issue we address in Section 4.2.

In Fig. 5, we consider the velocity distribution of satellites averaged over projected radii. Comparing real and redshift space samples, we see that the velocity errors and the redshift space distortions tend to broaden the velocity distribution. Applying the ‘ r_p cut’ to the redshift space mock slightly alters the shape of the velocity distribution (the number of satellites with smaller velocity difference is reduced more than those with larger velocity difference). The dependence of velocity dispersion on project radius seen in the mock might not occur in the real Universe. If so the incompleteness at small r_p has no effect and the 2dFGRS satellite samples can be interpreted as sampling the full velocity distribution within a given radius. However if the real satellites are like those in the mock we should restrict our comparisons to large scales where the ‘ r_p cut’ has no influence.

The velocity distribution of the mocks after applying the ‘ r_p cut’ is close to the one measured from the 2dFGRS. Both sets of satellite catalogues have a velocity distribution with an extended tail, with a nearly constant amplitude beyond ~ 800 km s $^{-1}$. This is to be expected due to contamination from interlopers and needs to be dealt with when analysing redshift space distributions.

At this stage we split the samples by absolute magnitude, as our theoretical prejudices, leads us to expect

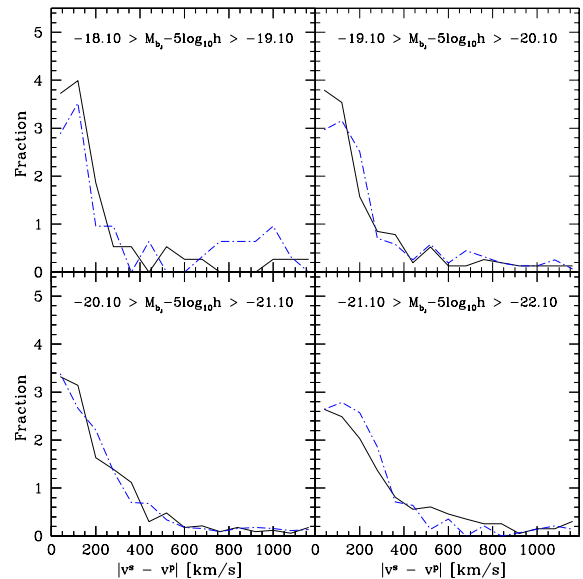


Figure 6. Velocity distributions of satellites within a projected radius of $400 h^{-1}$ kpc: similar plot as Fig. 5 (with same lines types showing 2dFGRS data and mock satellite sample in redshift space, with velocity errors and ‘ r_p cut’ applied), but split by absolute magnitude (indicated in each panel). The y-axis is here divided by the total number of satellites in each sample, to facilitate comparisons between samples of different sizes. For clarity, we omit errorbars. See text for discussion.

that the satellite velocity distributions will be more extended around brighter primaries. This is exactly what we see in the various panels of Fig. 6. The two top panels show the velocity distributions around the faintest primaries. For both samples, it seems clear that a velocity limit of 1200 km s $^{-1}$ is probably too large. Although not plotted the real space samples do not contain any galaxy with velocity $\Delta V \gtrsim 450$ km s $^{-1}$). Moreover, the faintest mock sample contains a ‘lump’ of galaxies at $\Delta V \sim 900$ km s $^{-1}$. This indicates that for faint primaries a smaller value for ΔV_s should be chosen, as otherwise contamination from interlopers will be very strong. The two bottom panels show the satellite velocity distributions around the brighter primaries. They both show the existence of satellite galaxies with large relative velocities, especially the brightest sample for which $\sim 20\%$ ($\sim 5\%$) of the satellites have a relative velocity larger than 500 km s $^{-1}$ (900 km s $^{-1}$). Therefore in order to measure the velocity dispersion of these systems it is essential to sample the full width of the velocity distribution.

We note that, with the exception for the brightest sample, the velocity distributions of the mocks are quite similar to those extracted from the 2dFGRS for each absolute magnitude split sample. For the brightest sub-sample the 2dFGRS velocity distribution is wider than that of the mock. We find that this is related to the presence bright ‘isolated’ ellipticals which are found in 2dFGRS sample. We address the influence of the morphological mix in section 5.2.

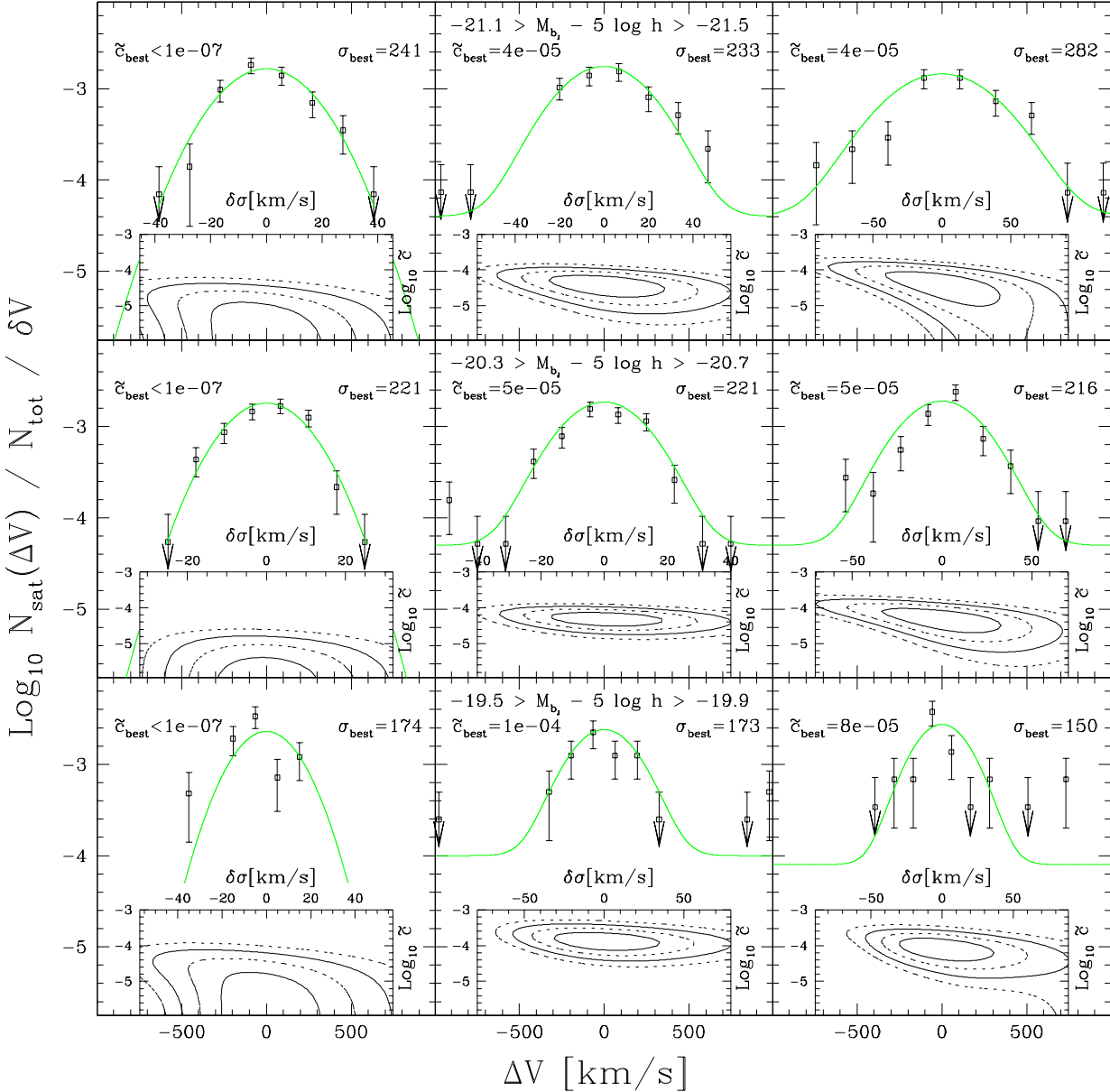


Figure 7. Fitting a Gaussian plus constant to the velocity distribution of satellite galaxies around primaries of three different absolute magnitude bins (bright to faint from top to bottom, with magnitude range indicated in the middle column) taken from respectively the mock satellite samples in real and redshift space and from the 2dFGRS data (from left to right). The binned satellite velocity distribution is shown by the squares with errorbars (assuming Poisson statistic) and the smooth curve the best fitting Gaussian plus constant, as determined by solving Eq. 4. The binning used is regular and of width $3/4 \sigma_{\text{best}}$, which, given in each panel, is the best velocity dispersion estimate, expressed in km s^{-1} . Intervals without bins represent velocity intervals without any satellites in. The best fit constant, \tilde{c} , is also given in s km^{-1} . The insets in each panel show, in dotted, the 1 and 2- σ contour levels, in the $\delta\sigma - \log_{10} \tilde{c}$ plane, of the two parameter fit and, in solid, the corresponding one parameter confidence contours. We point out that the velocity dispersion error contours are relative to σ_{best} and that insets in different panels have different scales. See text for further details.

4.2 Interlopers and Background Subtraction

In the previous section, we came across one important concern for the satellite sample: its contamination by interlopers. The core of the velocity distributions shown in Figs. 5 and 6 are rather well described by Gaussian distributions,

with some extended tails. These tails are due to interlopers, i.e. galaxies which in redshift space just happen to come within the selection region, but which in real space are more distant and belong to another halo/system.

Our stacked systems are probing a cylindrical volume

in redshift space. Hence to first order we would expect the interlopers to be randomly distributed within this cylinder. This motivates modelling the velocity distribution of each stacked system as the sum of a Gaussian and a constant. More precisely we set up a maximum likelihood estimator based on the following probability function:

$$p(v) = \frac{f(v)}{\int_{-v_{\text{fit}}}^{+v_{\text{fit}}} f(v) dv}, \quad (2)$$

$$f(v) = \frac{1}{\sqrt{2\pi}\sigma} \exp\left(-\frac{v^2}{2\sigma^2}\right) + \tilde{c}, \quad (3)$$

where the velocity fitting range is between $-v_{\text{fit}}$ and v_{fit} . Hence the maximum likelihood estimator is just the product of the probabilities $p(v_i)$ associated with each satellite, which can be written as:

$$\ln[\mathcal{L}] = -2 \sum_{i=1}^N \ln [f(v_i)] + 2N \ln \left[1 - \text{erfc}\left(\frac{v_{\text{fit}}}{\sqrt{2}\sigma}\right) + 2v_{\text{fit}}\tilde{c} \right]. \quad (4)$$

By maximising this likelihood as function of σ and \tilde{c} for each sample of stacked primaries, we are able to determine a typical velocity dispersion for these systems, together with the fraction of interlopers. We note that this approach can be applied to any subsample of satellite galaxies. Hence, we can, for example, test for a radial dependence of the satellite velocity dispersion by just considering satellites in different projected radial shells. The σ we measure in this way will be the underlying velocity dispersion of the stacked satellite system added in quadrature with the rms error of the measured satellite-primary velocity difference. This simple subtraction would only be invalid if the measured satellite-primary velocity differences were correlated with the measurements errors and there is no evidence for this in the 2dFGRS.

In Fig. 7, we show the results of this method for three magnitude bins (bright to faint from top to bottom) taken from the mock satellite samples in real (left) and redshift space (middle) and from the 2dFGRS data (right hand column). Note that we have not subtracted in quadrature the ‘known’ velocity measurement error, which for the data and the simulation is $v_{\text{err}} \sim 110 \text{ km s}^{-1}$ (see section 5.2), from the fitted velocity dispersion. The inset in each panel shows the 1 and 2- σ confidence regions³: as dotted contours for two free parameters (i.e. $\Delta\chi^2 = 2.30, 6.17$) and as solid contours for one free parameter (i.e. $\Delta\chi^2 = 1.0, 4.0$). As expected, the real space samples (i.e. left most column of Fig. 7) are all fit by a pure Gaussian, as in real space we do not have the problem of interlopers. The interloper fraction averaged over the fitted range is given by

$$I(\sigma, \tilde{c}) = \frac{2\tilde{c}v_{\text{fit}}}{\int_{-v_{\text{fit}}}^{+v_{\text{fit}}} f(v) dv} \quad (5)$$

and for the samples in redshift space we find a roughly constant value. For galaxies in the range $-20.3 \geq M_{\text{bj}} - 5\log_{10}h \geq -20.7$, and assuming a cylinder depth of

³ Assuming Gaussian errors, the likelihood given by Eq. 4 is distributed like a χ^2 distribution with two degrees of freedom (σ, \tilde{c}).

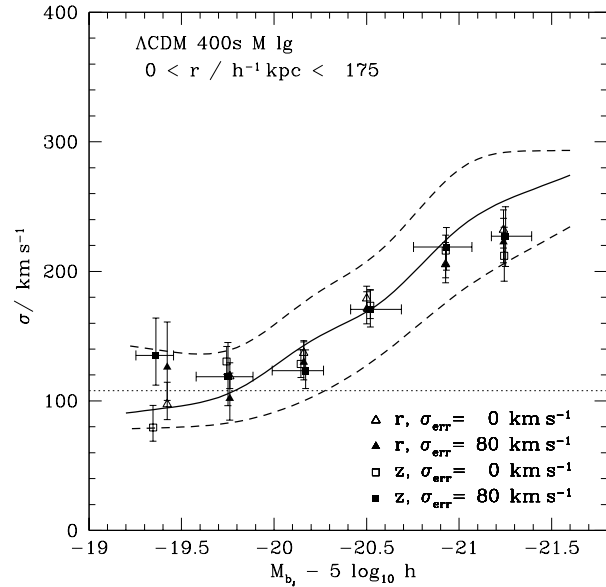


Figure 8. Velocity dispersion of ‘stacked’ primaries of given absolute magnitude for various mock samples: in real space with and without velocity errors included (filled and open triangles respectively) and in redshift space with and without velocity errors included (filled and open squares respectively). The errorbars plotted are the 1- σ errors as obtained from the 2 parameter fits on samples taken with cylinder depths of $\delta V = 1200 \text{ km s}^{-1}$, for samples brighter than M^* , and with cylinder depths of $\delta V = 600 \text{ km s}^{-1}$, for the fainter samples. The solid line is the median satellite velocity dispersion, as estimated from the volume limited semi-analytic galaxy catalogue. The two dashed lines shows the 16th and 84th percentiles of the velocity dispersion distribution. For samples where the 80 km s^{-1} velocity uncertainty has been included, we subtract from the estimated velocity dispersion the total velocity uncertainty, v_{err} , in quadrature. See text for discussion.

1200 km s^{-1} , we find interloper fraction of $10.7_{-2.4}^{+3.7}\%$. Interestingly the interloper fraction in the mock samples and the 2dFGRS data are similar for all the three magnitude bins presented in Fig. 7. This is another example of how well our mock catalogues mimic the real data.

Finally, we note that the size of the error on the satellite velocity dispersion differs between the mock and 2dFGRS samples. The typical 1- σ uncertainty on σ for the 2dFGRS data is approximately 30 km s^{-1} , independent of the best fitted velocity dispersion, whereas for the mock samples uncertainty is closer to 20 km s^{-1} . This is probably related to the greater homogeneity of mock catalogues, which, despite their high level of sophistication, do not contain as much variety as the real 2dFGRS data (see section 5.2).

5 VELOCITY DISPERSION OF SATELLITE SYSTEMS

We can now estimate the velocity dispersion of satellites around stacked primaries for different ranges of absolute magnitude within a chosen limiting transverse radial separation. The limiting radius needs to be large enough so that the composite satellite system contains sufficient satellites, but

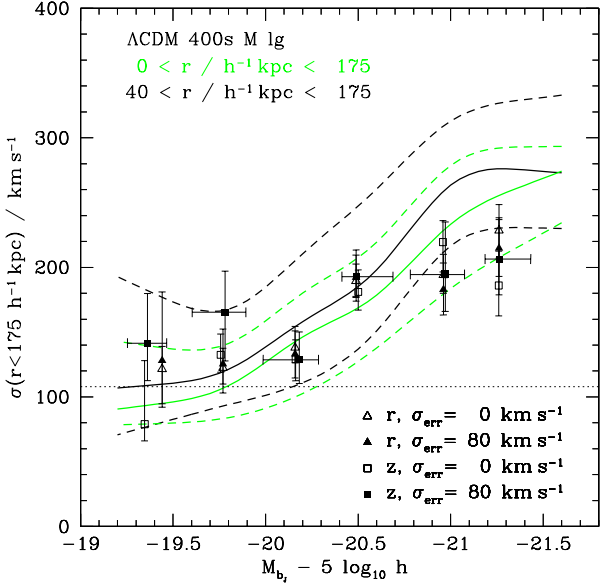


Figure 9. Velocity dispersion of ‘stacked’ primaries of given absolute magnitude for various mock samples: same as Fig. 8, but with the ‘ r_p cut’ applied. In light grey, we plot, as for reference, the same lines as shown in Fig. 8.

small enough so as to only sample dynamically connected regions. From theoretical considerations, a limiting radius of $175 h^{-1}$ kpc is reasonable for halo masses between 5×10^{11} and $10^{13} h^{-1} M_\odot$, as it is smaller than their typical virial radius, but still large enough to sample a fair fraction of the virial volume. Unless otherwise specified, our measurements are all done within a projected separation of $175 h^{-1}$ kpc from the primary.

5.1 Mock Satellite Velocity Dispersion

In Fig. 8, we plot the estimated velocity dispersion from the mock satellite samples in real (triangles) and redshift (squares) space, with and without velocity errors included (filled and empty symbols respectively). All are in pretty good agreement with the distribution of velocity dispersions measured directly from the full semi-analytic simulation cube, whose median and associated 16 and 84 percentiles are shown by the solid and dashed curves respectively. We note that when the volume limited simulation cube is analysed in this way including or excluding the most central satellites has a systematic effect on the measured velocity dispersion. Discarding all satellites within a projected radius of $\sim 5 h^{-1}$ kpc of the primary, results in a velocity dispersion which is systematically larger, by 5 to 15%.

Fig. 9 is like Fig. 8, but with the ‘ r_p cut’ applied to the samples analysed from both the simulation cube and mocks. For this reason, the black solid and dashed curves in Fig. 9 are slightly different to those in Fig. 8 (reproduced in grey in Fig. 9). The agreement between the various velocity dispersion estimates is not as good as in Fig. 8. Nevertheless, the satellite velocity dispersion inferred after applying the ‘ r_p cut’ agrees within the (typically 50% larger) errors with those measured before this cut was applied. In other words,

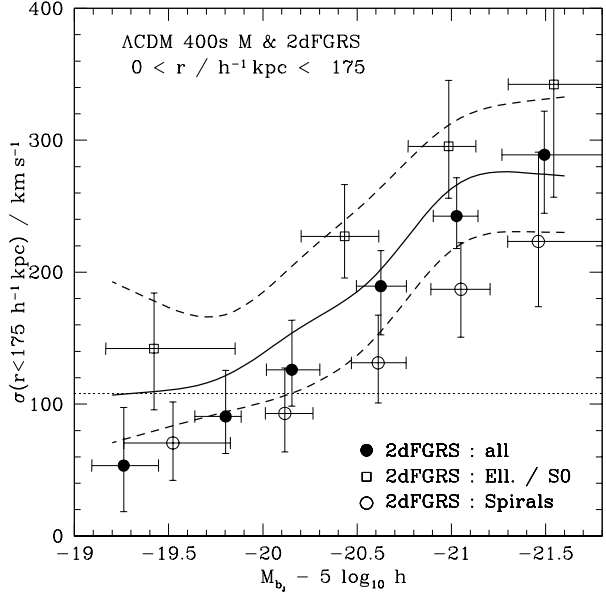


Figure 10. Velocity dispersion as measured using the isolation criterion as function of associated primary absolute magnitude. The data sample is shown for all primary types (filled solid circles), but also split by primary galaxy morphology: elliptical-S0 (open squares) and spiral-irregulars (open circles). The solid and dashed lines, same lines as shown in Fig. 9, are plotted here for comparison purpose only. See text for discussion.

the velocity dispersion as measured from satellite galaxies is not too sensitive to the innermost spatial distribution. This is probably not a big surprise, because of the mixed selection effects that come into the isolation criterion. Despite the less than perfect agreement between the simulation and mock in Fig. 9, it is important to have demonstrated that the velocity dispersion inferred from satellite galaxies is in general agreement with the median halo velocity dispersion measured in the simulation. However, the fact that the agreement is not perfect should also not be forgotten when interpreting the results of dynamical studies of stacked satellite systems.

We recall that to arrive at the velocity dispersion estimates plotted as the filled triangles in Figs. 9 and 8 we have subtracted in quadrature the mean velocity measurement error $v_{\text{err}} \sim 110 \text{ km s}^{-1}$, which comes from adding in quadrature the velocity measurement errors of primaries and the satellites. This has the desired effect of producing estimates that are all in reasonable agreement with each other, but also has the consequence that the fractional error on the estimated velocity dispersion is increased by a factor $\sigma / (\sigma^2 - v_{\text{err}}^2)^{1/2}$ relative to that of the σ that comes from the maximum likelihood algorithm. Nevertheless, Figs. 8 and 9 show that for nearly the full absolute magnitude range covered by our data we are able to recover the underlying velocity dispersion without any strong biases due to selection effects.

5.2 Satellite Velocity Dispersion from 2dFGRS

For the 2dFGRS satellite sample, we find it useful to split the sample based on whether the primary is an isolated spiral or

elliptical galaxy. In Fig. 10, we plot the velocity dispersions for the combined 2dFGRS samples (filled circles) as well for the subsets of satellites with spiral (and irregular) primaries (open circles) and elliptical-S0 primaries (open squares). In the mocks, if we infer the morphological types of the primaries from the bulge-to-disk ratios, then we also find a small fraction of elliptical primaries. However, the correspondence between bulge-to-disk ratio and morphology is crude and so we prefer not to split the mock sample in this way. Fig. 10 shows that the velocity dispersions from the mocks are in very good agreement with those from the overall 2dFGRS sample, but we also see in the 2dFGRS that the velocity dispersions of satellites around spiral primaries are significantly lower than those of satellites around elliptical primaries.

We also note that for the 2dFGRS the typically error on the estimated velocity dispersion is twice as large as in the corresponding mock sample. This is most certainly related to a combination of the following factors: the mock satellite samples are typically two times larger than the two 2dFGRS satellite samples (as the mock catalogues used are not split by morphology); due to the limited physics included the mock samples are likely to be more statistically homogeneous than the real data; the average number of satellites per primary is slightly smaller in the data than in the mocks and the smaller total number of satellites in the data will lead to more scatter in the estimated velocity dispersion.

Based on the correspondence between the estimated satellite velocity dispersions and those of the underlying dark matter haloes found for the mocks in Section 5.1, we make the claim that the velocity dispersions of the primaries as inferred from the 2dFGRS satellite sample should be a reliable tracer of the primaries ‘true’ velocity dispersions. Quantitatively, we expect this method to work for ‘isolated’ galaxies brighter than $M_{b,J} - 5\log_{10}h \simeq -19.0$, i.e. galaxies which are as bright or brighter than the Milky-Way.

6 MASS ESTIMATE OF ISOLATED SYSTEMS

In section 5, we showed that it is possible, over a range of absolute magnitudes, to recover from the satellite velocity dispersion the underlying halo velocity dispersion. Therefore, it is tempting to go one step further and infer the mass which is dynamically enclosed in these systems. There are, nevertheless, many issues which needs to be dealt with in order to obtain a reliable mass estimate. Two major concerns are, of course, which mass estimator to use and how to choose the radius within which to measure the mass. Our approach is to calibrate a mass estimator using the mocks, as for them we know the mass of the parent dark matter halo of each galaxy.

6.1 Calibration of mass estimator

The way we calibrate the halo mass-luminosity relation is to measure in the simulation the relation between halo mass and halo velocity dispersion and so obtain a way to relate the measured velocity dispersion to a halo mass. In Fig. 11, we plot the satellite velocity dispersion as measured in the volume limited semi-analytic catalogue as function of the associated halo mass within $175 h^{-1}$ kpc, M_{175} . The varying

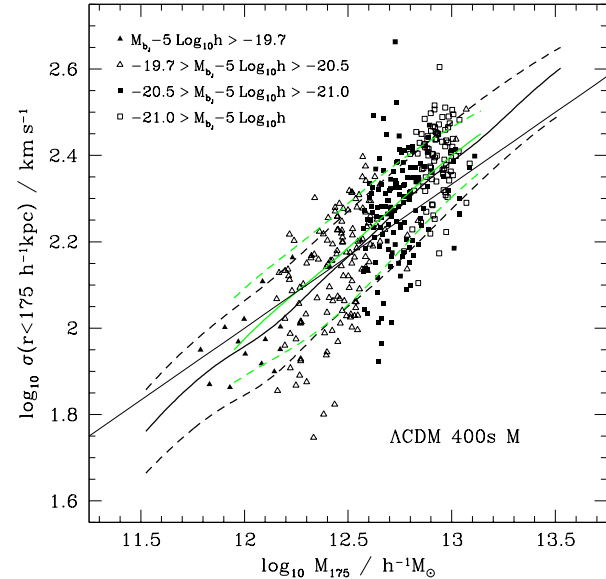


Figure 11. Satellite velocity dispersion in the volume limited mock catalogue as function of the associated primary halo mass. Both the halo mass and the satellite velocity dispersion are measured within a radius of $175 h^{-1}$ kpc. The different symbols correspond to isolated systems found in the mock survey and labelled as function of primary luminosity (see key). The thick grey and black solid lines correspond to the median satellite velocity dispersion as measured from the simulation cube for all primaries found in the mocks and all central galaxies in the simulation cube respectively. The associated dashed line corresponds to 16th and 84th percentiles of the satellite velocity dispersion distributions. For comparison purpose the median dark matter velocity dispersion is also plotted as a thin black line.

symbol type indicates the absolute magnitudes of the isolated primaries (see the figure legend). The galaxy formation model used preserves very accurately the mass-luminosity hierarchy of central galaxies⁴. By this we mean not only that on average bright central galaxies reside in massive halos and faint central galaxies in the less massive ones, but also that the scatter in this whole mass-luminosity relation is quite small. This is an essential assumption which needs to be accurately satisfied both in the model and the genuine data for the method of stacked primary systems to work.

Mocks created from the same dark matter simulation, but with the Cole et al. (2000) galaxy formation model have a much larger scatter in the relationship between halo mass and central galaxy luminosity and can therefore not be used in the calibration process. The scatter present in those mocks does not allow satellites of primaries of similar luminosity to be stacked, as they can belong to systems which are intrinsically too different in mass. Since this work began, a whole new suite of semi-analytic galaxy formation models with AGN feedback have appeared (e.g. Croton et al. (2005), Bower et al. (2006)). These models also have quite a

⁴ This is only true for halo masses with circular velocities below 400 km s^{-1} , as for halos with larger circular velocities, an artificial cut-off in the cooling recipe creates much fainter central galaxies in the very largest halos.

large scatter in the relationship between halo mass and primary luminosity, though less than in the Cole et al. (2000) semi-analytic model. We simply restate that by stacking systems by primary luminosity and then attempting to infer the halo mass, we are implicitly assuming that the scatter between luminosity and mass is small and so in calibrating such a relation we should use a mock catalogue in which this is true.

Using Springel et al. (2001) semi-analytic model of galaxy formation in the full simulation cube, we show in Fig. 11 that using all central galaxies or just those whose primaries satisfy the isolation criterion make very little difference to the relation satellite velocity dispersion and dark matter halo mass. In both cases the medians and the 16th and 84th percentiles of the satellite velocity dispersion distributions match well over one full magnitude in halo mass. They are both well parametrised by a power-law relation of the form $\sigma_{175} \propto (M_{175})^\alpha$, with α ranging between ~ 0.42 and ~ 0.56 , depending on which percentile of the velocity dispersion distribution one attempts to fit. We note that in our mock we do not find any isolated systems residing in halos outside the range $\sim 5 \times 10^{11} h^{-1} M_\odot \sim 10^{13} h^{-1} M_\odot$. Hence any mass estimate outside this range is based on assuming the good correspondence found in Fig. 11 around isolated halos and central galaxies holds over a larger mass range. Finally, we have investigated whether the calibrating relation in the mocks is the same for both elliptical and spiral primaries. For our crude bulge-to-disk ratio assignment of morphological type we find the relations are virtually identical and so we have opted to use the one overall relation present in Fig. 11 in all cases.

6.2 Mass estimates for 2dFGRS primaries

We now use the relation between the median velocity dispersion of all central galaxies and halo mass, shown in Fig. 11, to directly convert the measured satellite velocity dispersions into estimates of halo masses. In Fig. 12, we plot the estimated masses for primaries split by morphological type. As is to be expected, we find in both cases that the inferred halo mass increases steadily with the absolute magnitude of the primary. With this mass calibration, we find that elliptical galaxies live in halos which are typically 3 to 10 times more massive than spirals of similar b_J brightness.

The scatter seen in Fig. 11 indicates that the uncertainty in the mass calibration is large. For a given halo mass, the scatter in velocity dispersion is around ~ 25 to $\sim 40\%$. Hence, considerable care should be taken when using this relation to infer halo mass from the measured velocity dispersion. In Fig. 12, we are assuming that the satellite velocity dispersion measurement inferred from the 2dFGRS is in good agreement with the median of the ‘true’ satellite velocity dispersion. In Fig. 8, we showed that for the mocks the corresponding agreement is good, but not perfect. For the mocks we can use the spread between 16th and 84th percentiles of the distribution as a guide to the uncertainty in this calibration and hence on the the systematic uncertainty in the calibration procedure. For an individual object, a systematic shift of $\sim 75\%$ in the estimated mass is entirely acceptable, as this shift corresponds to the 1- σ dispersion on the calibration relation.

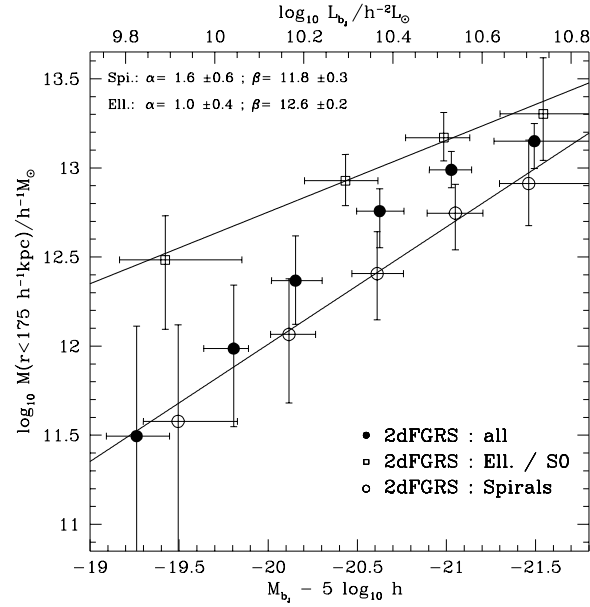


Figure 12. Simulation calibrated halo mass, within $175 h^{-1}$ kpc, as function of primary absolute magnitude. The open squares corresponds to the mass of the halos of elliptical galaxies, whereas open circles to spiral halo masses. The solid dots corresponds to the halo mass of an ‘average’ galaxy. The errorbars plotted do only take into account the error on the measured velocity dispersion. Errors due to uncertainties in the mass-velocity dispersion calibration are not taken into account (see text for further details). The best fit parameters for the mass-luminosity relation given by Eq. 6 are given for spirals and ellipticals, and plotted as solid lines.

Using this calibration, we find the power-law fit relation

$$\frac{M_{175}}{h^{-1} M_\odot} = \left(\frac{L_{b_J}}{L_*} \right)^\alpha \left(\frac{M_*}{h^{-1} M_\odot} \right) \quad (6)$$

between the halo mass within $175 h^{-1}$ kpc, M_{175} , and the b_J -band luminosity of the primary, L_{b_J} . This can be written equivalently as

$$\log_{10} [M_{175} / (h^{-1} M_\odot)] = \alpha \log_{10} [L_{b_J} / L_*] + \beta, \quad (7)$$

where L_* is the characteristic luminosity as given by the 2dFGRS Schechter luminosity function estimate of Norberg et al. (2002), and $\beta = \log_{10} [M_* / (h^{-1} M_\odot)]$, with M_* the dynamical mass of an L_* galaxy. For elliptical galaxies, we observe a nearly linear relation between halo mass and luminosity, with $\alpha \simeq 1.0 \pm 0.4$ and $\beta \simeq 12.6 \pm 0.2$, i.e. a nearly luminosity independent mass-to-light ratio. This is in stark contrast with spiral galaxies, for which the relation between halo mass and primary luminosity is much steeper, with $\alpha \simeq 1.6 \pm 0.6$ and $\beta \simeq 11.8 \pm 0.3$. The errors on these best fit parameters are, as already mentioned, rather substantial.

We note that the existence of a difference between the scaling relations for ellipticals and spirals is independent of the calibration used. The calibrating relation between halo mass and satellite velocity dispersion was assumed to be independent of galaxy morphology and hence the difference in the mass-luminosity scaling relations is due entirely to the differences in the measured luminosity - velocity dispersion

relations. However the magnitude of this difference does depend on the halo mass-velocity dispersion calibration used.

Finally, for a spiral galaxy like the Milky-Way we estimate the halo mass within $175 h^{-1}$ kpc to be approximately $3.5_{-2.1}^{+4.0} \times 10^{11} h^{-1} M_{\odot}$, whereas for an elliptical galaxy of similar b_J brightness we estimate its halo mass to be nearly eight times larger. We note the large statistical error associated to this mass estimate, which do not include any systematical error on the mass calibration relation used.

6.3 Comparison with other mass estimates

This statistical Milky-Way mass estimate needs to be compared with other Milky-Way mass estimate, using completely different techniques. When comparing with techniques independent of the value of the Hubble constant, we assume here $H_0 = 70 \text{ km s}^{-1} \text{ Mpc}^{-1}$, implying our estimate of the Milky-Way mass within 250 kpc becomes $5.0_{-3.0}^{+5.7} \times 10^{11} M_{\odot}$. Assuming a simple scaling relation for the mass enclosed at large radii (e.g. $M(r) \sim r$, isothermal sphere), we estimate the mass within 100 kpc to be $2.0_{-1.2}^{+2.3} \times 10^{11} M_{\odot}$.

From the dynamics of the Magellanic Clouds and the associated stream, Lin, Jones, & Klemola (1995) estimate the mass of the Milky Way inside 100 kpc to $(5.5 \pm 1) \times 10^{11} M_{\odot}$. From the escape velocity and motions of satellite galaxies, Kochanek (1996) estimates the mass of the Galaxy inside 100 kpc to be $(5 - 8) \times 10^{11} M_{\odot}$. Using more recent kinematic information for Galactic satellites and halo objects, Sakamoto, Chiba, & Beers (2003) derive an essentially model independent Galaxy mass estimate within ~ 50 kpc of $5.5_{-0.2}^{+0.1} \times 10^{11} M_{\odot}$, which corresponds to $\sim 10^{12} M_{\odot}$ within 100 kpc. This mass, which is nearly twice as large as the one found by Lin et al. (1995), seems to be confirmed by Bellazzini (2004), who uses the tidal radii of remote globular clusters (between 35 and ~ 200 kpc from the Galactic Centre) to provide constraints on the mass profile of the Milky Way, independently of kinematic data and yielding an enclosed mass of $1.3_{-1.0}^{+2.9} \times 10^{12} M_{\odot}$ at ~ 90 kpc.

All these estimates are at least a factor of two larger than our estimate and the more recent Milky-Way mass estimates are as much as a factor 5 larger. There are several systematic effects that could be contributing to this difference. Firstly, our estimate is a statistical estimate of the mean mass for galaxies of a given luminosity. The scatter about this mean relation is large and ought to be taken into account. For instance, the scatter of the halo mass satellite velocity dispersion calibration relation is 25% for a given mass, which translated into the mass luminosity relation implies a typical 75% scatter for a given luminosity. Secondly, our mass estimate for the Milky-Way is obtained using a power-law fit to the data, which therefore averages data over a range of luminosities. If a power-law is not appropriate and only the data in a bin centred at the Milky-Way's luminosity were used then the statistical error on our estimate would be $\sim 70\%$ larger. Finally, according to the Milky-Way models of Kochanek (1996), the assumption of isothermal sphere between 100 kpc to 250 kpc may not be appropriate. Following his figure 7, the scaling is closer to $M(r) \sim r^{0.6}$, implying a $\sim 50\%$ increase in the estimated Milky-Way mass.

Taking these statistical and systematic issues into account, our mass estimate is compatible with those of Lin et

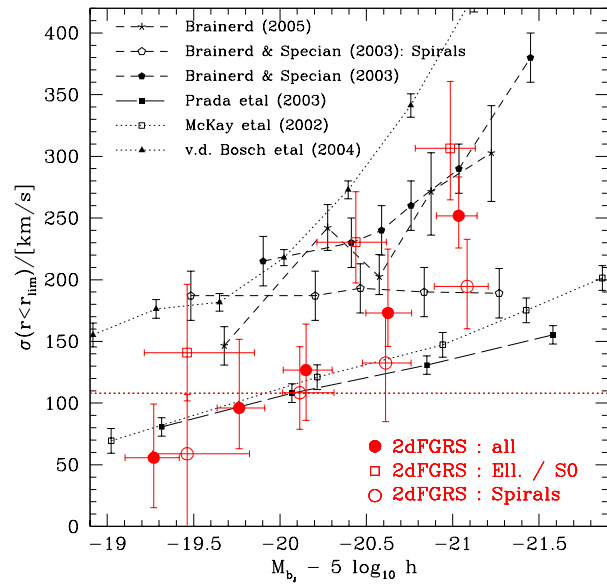


Figure 13. Comparison of velocity dispersion estimates as function of absolute magnitude from recent analyses using similar techniques. For Prada et al. (2003), McKay et al. (2002a), Brainerd & Specian (2003) and Brainerd (2005), the quoted errorbars are upper limits on the errorbars shown in their respective analyses. For van den Bosch et al. (2004), we show their final velocity dispersions estimates, for their satellite sample optimised so as to have, according to mock catalogues constructed using the conditional luminosity function, the lowest amount of interlopers. Our measurements, within $175 h^{-1}$ kpc, are the same as presented in Fig. 10. See section 7, but also the Appendix A, B and C for further comments on this rather busy plot.

al. (1995) and Kochanek (1996), but still roughly a factor of 2-3 too small when compared to the recent estimates from Sakamoto et al. (2003) and Bellazzini (2004). Clearly our statistical method is not optimal for inferring the mass of an individual object. A fairer comparison would be to compare our results with other statistical mass estimators, like McKay et al. (2002) did when comparing with weak lensing estimates from SDSS (McKay et al. 2001).

7 COMPARISON TO SIMILAR METHODS

There have recently been several complementary studies that have used similar techniques to stack satellites around isolated primaries (McKay et al. 2002; Prada et al. 2003; Brainerd & Specian 2003; van den Bosch et al. 2005; Brainerd 2005). The results of these studies, appropriately converted into $M_{b_J} - 5 \log_{10} h$ where necessary, are compared to ours in Fig. 13. At first sight, one sees very large variation between the findings of the different authors. However one has to be very careful because both the selection criteria and method of estimating velocities vary considerably. A more detailed comparison between the different analysis methods is presented in the Appendices. The tests presented there show why some estimates differ, but also raise new concerns over other estimates which on face value appear to agree when in reality they probably should not.

From the analysis presented in the Appendix A, we learn first that the agreement in the results from McKay et al. (2002) and Prada et al. (2003) is, as already claimed by Prada et al. (2003), spurious. The selection criteria are different enough so that when applied to mocks the results are expected to be significantly different. It is clear from the paper of Brainerd & Specian (2003) that they have not subtracted the pairwise velocity measurement uncertainty from their velocity dispersion estimate, while Brainerd (2005) does take it into account. Despite this (see Appendix B), the results from Brainerd & Specian (2003) and Brainerd (2005) still do not agree with our findings also extracted from the 2dFGRS. We believe this is due to some source of extra contamination of their satellite sample, but we are unable to reproduce their results. Moreover, we find that the difference between our measurements and those of Prada et al. (2003) is mostly due to the different selection criteria used to define the samples. The larger errors on our 2dFGRS velocity dispersion estimates cannot be explained solely by the larger redshift measurement errors of the 2dFGRS data. Using the data of Prada et al. (2003), we find their quoted errors to be approximatively 30-40% smaller than those we estimate.

As a final conclusion from this comparative work, we have to point out that the large variety of results present in the literature reflects mostly the large variation in the proposed methods of both identifying the isolated systems and also measuring the satellite velocity dispersions. All the proposed methods introduce biases and unless one applies the same selection criterion to a set of realistic mock galaxy catalogues one cannot quantify these systematic effects and the interpretation of the results remain questionable.

8 CONCLUSIONS

We have developed, tested and applied a method to probe the properties of extended dark matter haloes around bright galaxies. We do this by carefully selecting isolated galaxies in the 2dFGRS and using their faint satellites as tracers of the gravitational potential. By stacking systems of similar primary luminosity to improve the signal-to-noise, we estimate the satellite velocity dispersion. Realistic mock galaxy catalogues, created from cosmological N-body simulations populated with a semi-analytic galaxy formation scheme, enable us to relate the measured velocity dispersion of the satellite system to the velocity dispersion and mass of the underlying dark halo.

Fig. 10 shows evidence for the existence of dark matter halos around typical galaxies. Our sample of satellites probes the potential well of the primaries out to several hundred kiloparsecs and demonstrates that the dark halos extend many times beyond the optical radius of the primary. This is in agreement with the current theoretical picture of galaxy formation in a cold dark matter universe (e.g. White & Frenk 1991, Kauffmann et al. 1993, Cole et al. 2000). The satellite velocity dispersion increases with the luminosity of the primary and is much larger for elliptical galaxies than for spiral galaxies of similar b_J luminosity.

The total extent of the dark halo is not constrained by our data. Although, the satellite distribution extends to $r_p \sim 375 h^{-1}$ kpc, most of the signal comes from within

$r_p \sim 175 h^{-1}$ kpc. Within the errors, the velocity dispersion appears to be constant within $r_p \sim 175 h^{-1}$ kpc and $r_p \sim 375 h^{-1}$ kpc. In this range, the satellite velocity dispersion does not depend strongly on the luminosity of the primary.

Our mock catalogues allow us to calibrate the velocity dispersion-mass relation for galaxies selected according to the isolation criterion of our 2dFGRS sample. Fig. 12 then indicates that elliptical galaxies reside in haloes which are at least 4 times more massive than spiral galaxies of similar b_J brightness. Galaxy like the Milky-Way typical reside in dark matter halos of mass $\sim 3.5^{+4.0}_{-2.1} 10^{11} h^{-1} M_\odot$ within $175 h^{-1}$ kpc.

A key assumption in our analysis is that isolated galaxies of similar luminosity reside in halos of similar mass. It is this that justifies the stacking procedure. Our semi-analytic models allow us to test the validity of this assumption. We find that in one of two semi-analytic models that we have investigated, the Springel et al. (2001) model, there is very little scatter in the relation between central galaxy luminosity and halo mass. A different semi-analytic model, however, that by Cole et al. (2000), predicts considerable scatter in this relation and this introduces large errors in the halo properties inferred from a stacking analysis. Mocks constructed from this model return an increasing satellite velocity dispersion as a function of primary luminosity which, however, deviates systematically from the velocity dispersion of the host dark halos. The reasons behind this difference in the galaxy formation models are not investigated in detail here but it serves to illustrate that significant theoretical uncertainties remain in the kind of analysis that we have presented here.

ACKNOWLEDGEMENTS

We thank Tim McKay for a very helpful referee's report. The 2dFGRS was carried out using the 2 degree field facility on the 3.9m AngloAustralian Telescope (AAT). We thank all those involved in the smooth running and continued success of the 2dF and the AAT. During the far too long course of this work, PN acknowledges funding from the Swiss National Science Foundation (TMR PhD Grant), an ETH Zwicky Fellowship, a PPARC fellowship at the IfA, as well as a visitor status at the ICC and many stimulating discussions with Felix Stoehr, Simon White, Liang Gao, Cristiano Porciani, Frank van den Bosch, Diego Lambas and Francisco Prada. CSF acknowledges a Royal Society Wolfson Research Merit award.

REFERENCES

- Bellazzini M., 2004, MNRAS 347, 119
- Brainerd T.G., Specian M.A., 2003, ApJL 593, 7
- Brainerd T.G., 2005, ApJL 628, 101
- Cole S.M., Lacey C.G., Baugh C.M., Frenk C.S., 2000, MNRAS 319, 168
- Colless, M.M., et al. (the 2dFGRS Team), 2001, MNRAS 328, 1039
- Colless, M.M., et al. (the 2dFGRS Team), 2003, astro-ph/0306581

Dalton, G.B., Maddox, S.J., Sutherland, W.J., & Efstathiou, G., 1997, MNRAS, 289, 263.

De Lucia G., Kauffmann G., White S.D.M., 2004, MNRAS 349, 1101

Eke, V., et al. (the 2dFGRS Team), 2004, MNRAS 355, 769

Gao L., White S.D.M., Jenkins A., Stoehr F., Springel V., 2004, MNRAS 355, 819

Kauffmann, G., White, S. D. M., & Guiderdoni, B. 1993, MNRAS, 264, 201

Lin D.N.C., Jones B.F., Klemola A.R., 1995, ApJ 439, 652

Loveday J., 1996, MNRAS 278, 1025

Madgwick, D. S., et al. 2002, MNRAS, 333, 133

McKay, T., et al. , 2001 , ApJ submitted, astro-ph/0108013 (not published)

McKay, T., et al. , 2002 , ApJ, 571, L85

Norberg P., et al. (the 2dFGRS Team), 2002, MNRAS

Prada F., et al. , 2003, ApJ 598, 260

Rubin V.C., Ford W.K., 1970, ApJ 159, 379

Sakamoto T., Chiba M., Beers T.C., 2003, A&A 397, 899

Springel V., White S.D.M., Tormen G., Kauffmann G., 2001, MNRAS 328, 726

Stoehr, F., White, S.D.M., Tormen, G., & Springel, V., 2002, MNRAS 335L, 84

van den Bergh S., 1992, A&A 264, 75

van den Bosch F.C., Norberg P., Mo H.J., Yang X., 2004, MNRAS 352, 1302

van den Bosch F.C., Yang X., Mo H.J., Norberg P., 2005, MNRAS 356, 1233

White, S. D. M., & Frenk, C. S. 1991, apj, 379, 52

White S.D.M., Rees M.J., 1978, MNRAS 183, 341

York, D., et al. , 2000, AJ 120, 1579

Zaritsky, D., Smith, R., Frenk, C.S., & White, S.D.M., 1993, ApJ, 405, 464

Zaritsky, D., Smith, R., Frenk, C.S., & White, S.D.M., 1997a, ApJ, 478, L53

Zaritsky, D., Smith, R., Frenk, C.S., & White, S.D.M., 1997b, ApJ, 478, 39

APPENDIX A: COMPARISON WITH SATELLITE VELOCITY DISPERSION MEASUREMENTS FROM SDSS DATA

The studies of McKay et al. (2002) and Prada et al. (2003) are based on different releases of SDSS data. In Fig. 13, their results are shown by dot-connected open squares and by long-dashed connected filled squares respectively. At first sight their results appear in rather good agreement with each other, and rather different to ours, which are shown by large filled circles (all primaries), large open circles (spiral primaries) and large open squares (elliptical/S0 primaries). However, it is essential to consider the differences expected due to the differing satellite selection criteria.

A1 McKay et al.: $\delta m_s = 1.5$ & $\delta r_b = 2 h^{-1}\text{Mpc}$

McKay et al. (2002) (and also Prada et al. (2003) with their sample 3⁵) use a much less stringent isolation criterion on the neighbourhood of the primary. Our requirement for the primary to be at least 8 times more luminous than any of its satellites is relaxed to just 4 times brighter. We recall that the role of this constraint is to avoid including satellite

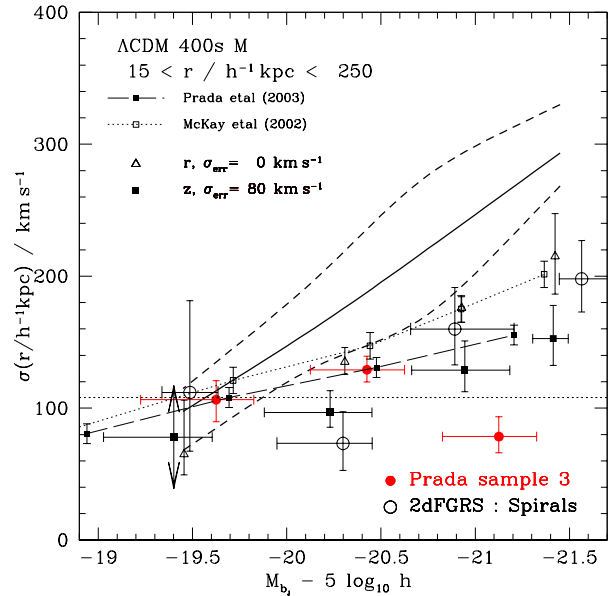


Figure A1. Comparison of velocity dispersion estimates as function of absolute magnitude, adopting the same criterion as McKay et al. (2002) and Prada et al. (2003) in their sample 3. The labelling is the same as in Fig. 13, with the exception that we have added our mock catalogue results (open triangles and filled squares for real and redshift space respectively) for this new isolation criterion, where the velocity dispersion is measured for satellites between 15 and 250 h^{-1} kpc using a cylinder depth of 500 km s^{-1} . The filled large points correspond to our measurement done on sample 3 of Prada et al. (2003). Note that the connected filled squares from Prada et al. (2003) are estimates using the selection criterion discussed in Fig. A2.

systems in which the potential well and hence the dynamics of the satellites is not dominated by the the primary. To avoid this being the case it is necessary to ensure that all the satellites are much less massive than the primary. The recent mass-to-light ratio measurements of Eke et al. (2004) indicate that for around $2 L^*$, which is the luminosity of our brighter primaries, a factor of 8 in luminosity corresponds to factor 10 in mass. However for lower luminosity primaries the corresponding mass factor is smaller and this argues for having a large luminosity difference between satellite and primary.

Another difference between our standard isolation criterion and the one used by McKay et al. is the much larger outer exclusion radius. Our requirement is to have all galaxies within $1 h^{-1}\text{Mpc}$ be at least 0.8 magnitudes fainter than the primary, whereas McKay et al. require for the same magnitude difference a distance of $2 h^{-1}\text{Mpc}$, which is certainly a more restrictive criterion.

Therefore in order to make the appropriate comparison, we need to apply the same selection criterion as McKay et al. (2002). Fig. A1 compares the results of McKay et al. (2002) with new estimates we have made from the 2dFGRS data after adopting their selection criterion. Also shown in Fig. A1 are velocity dispersion estimates we have made using sample 3 of Prada et al. (2003). Using the same selection criterion, we now find results which are in better agreement with the SDSS estimates, but with larger errorbars. There

⁵ This sample is presented in their paper, but is not the sample for which they derive their main results.

are two reasons why our errors are larger. Firstly, the much larger velocity uncertainty of 2dFGRS redshift measurements (typically 85 km s^{-1} on an individual galaxy for the 2dFGRS, compared to less than 30 km s^{-1} for SDSS) causes the errors from the maximum likelihood method to be increased by 50 %, for systems with a ‘true’ satellite velocity dispersion of 100 km s^{-1} , instead of just 7 % in the case of SDSS. Secondly, the errors quoted by Prada et al. (2002) are intrinsically smaller than those we obtain when performing our maximum likelihood estimation on their sample 2. This result can be partially explained if Prada et al. have assumed Poisson statistics to derive their quoted errorbars.

Comparing the results of applying this relaxed selection criterion to the mock catalogues, with the distribution of the underlying satellite velocity dispersions shown by the heavy solid and dashed lines in Fig. A1, we see that there is a large bias. The velocity dispersion recovered from the mocks lie outside the 16th to 84th percentile band of the ‘true’ underlying galaxy velocity distribution. In our analysis of the samples with relaxed isolation criterion we also note that for both the 2dFGRS data and the mocks the stacked satellite velocity distributions are no longer well fit by the ‘Gaussian plus a constant’ model. The samples look much more like the real space velocity distributions shown in Fig. 7, i.e. there is just an upper limit for the constant. In other words, with these satellite samples, fitting the 2dFGRS data with a ‘Gaussian plus a constant’ is not appropriate. On the other hand, the satellite velocity distribution of sample 3 of Prada et al. is well fit by a ‘Gaussian plus constant’. This indicates some clear difference between the two satellite samples.

A2 Prada et al.: $\delta m_b = \delta m_s = 2.0$ & $\delta r_b = 0.5 h^{-1}\text{Mpc}$

The selection criterion proposed by Prada et al. (2003) are more conservative than those of McKay et al. (2002), as they require a factor of ~ 6 in luminosity between the primary and any of the surrounding galaxies. However, for the spatial isolation of the primary, Prada et al. are much less restrictive with an outer isolation radius, δr_b , of $0.5 h^{-1}\text{Mpc}$, compared to $2 h^{-1}\text{Mpc}$ for McKay et al. (2002). Compared to our choice, this criterion is less restrictive, especially as we require within $\delta r_s = 0.5 h^{-1}\text{Mpc}$ a factor of 8 in luminosity difference, and within $\delta r_b = 1 h^{-1}\text{Mpc}$ the primary to be at least twice as luminous as any other galaxy. However, this is not the only difference between the two SDSS satellite analyses. The biggest difference is that Prada et al. fit for the satellite velocity dispersion and interloper fraction separately in each bin of projected radius. Thus they allow both the interloper fraction and velocity dispersion to vary with projected radius.

Including this extra freedom in their velocity dispersion calculations gives rise, as we show in Fig. A2, to a substantial difference in the velocity dispersion estimates, compared to what is found in Fig. A1, using the analysis method proposed by McKay et al. (2002). From Fig. A2, we conclude that satellite velocity dispersion estimates from 2dFGRS and SDSS (using sample 2 of Prada et al. 2003) agree with each other and that the criterion and method used seem to be able to recover (within its large uncertainties) the underlying velocity dispersion, which is not the case for the method of McKay et al. (2002). Finally we are able,

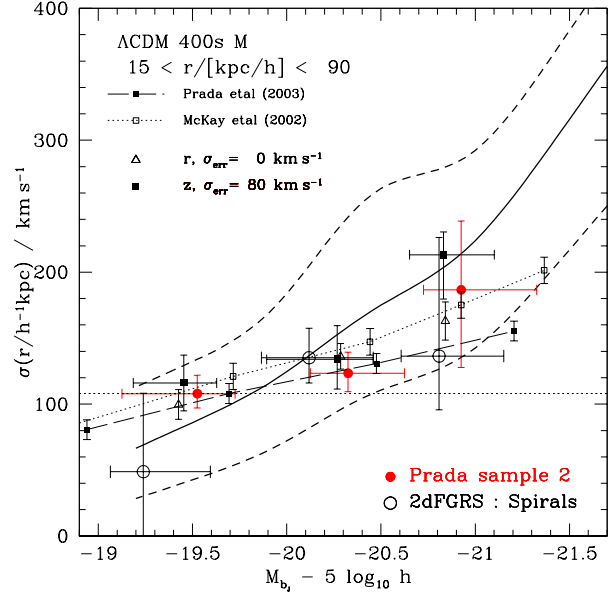


Figure A2. Comparison of velocity dispersion estimates as function of absolute magnitude, adopting the same criterion as used by Prada et al. (2003). The labelling is the same as in Fig. 13, with the exception that we have added our mock catalogue results (open triangles and filled squares for real and redshift space respectively) for this new isolation criterion, where the velocity dispersion is measured for satellite between 15 and $90 h^{-1} \text{ kpc}$ using a cylinder depth is 500 km s^{-1} . The filled large points correspond to our measurement done on sample 2 of Prada et al. (2003). Note that the dot-connected open squares from McKay et al. (2002) are obtained with the selection criterion discussed in Fig. A1.

but with larger errors, to recover the velocity dispersion estimates found by Prada et al. (2003). Only for the brightest galaxies is there any indication of a discrepancy, and this is mainly related to error estimates from Prada et al. (2003) which for those samples are clearly much smaller than we find.

Regarding the statistics of the isolated satellite systems, we note that adopting the selection criterion of Prada et al. (2003) causes the number of systems with at least 6 satellites within $250 h^{-1} \text{ kpc}$ to increase drastically. This statistic is similar to the one we used before, i.e. at least 9 satellites within $400 h^{-1} \text{ kpc}$, to identify and remove small groups from our sample. Table A1 compares these statistics for the 2dFGRS data for our original selection criterion, those of Prada et al. (2003) and those of McKay et al. (2002). Typically the Prada et al. (2003) selection criterion results in twice as many ‘large systems’ as for our standard selection criterion, independent of the value of N_{viol} and ΔV_s used. Hence the sample of primaries might not be as well isolated as one hopes. Interestingly, as long as $N_{\text{viol}} = 0$, the selection criterion of McKay et al. are very comparable to ours as regards the number of ‘large systems’ identified. Nevertheless, we note that in all cases the fraction of satellite galaxies that are in these ‘large systems’ is always small.

Table A1. Properties of the combined NGP & SGP satellite samples around bright galaxies, for two values of N_{viol} and for different selection criteria, as indicated by δm_s and ΔV_s . The McKay et al. selection criterion correspond to $\delta m_s = 1.5$, Prada et al. to $\delta m_s = 2.0$ and ours to $\delta m_s = 2.2$. All satellites are within $250 h^{-1}$ kpc from the primary. The columns labelled ‘large systems’ indicate how many primaries and satellites are found in systems with 6 or more satellites within $250 h^{-1}$ kpc. The last 3 columns show the total number of satellites within two cylindrical shells, where r_p is expressed in h^{-1} kpc. These numbers include the satellites belonging to ‘large systems’.

δm_s	ΔV_s	N_{viol}	N_{prim}	N_{sat}	large systems		N_{sat}	$15 < r_p < 90$	$90 < r_p < 250$	$15 < r_p < 250$
					N_{prim}	N_{sat}				
2.2	600	0	299	425	3	21	289	133	289	422
2.0	600	0	513	754	7	52	499	244	499	743
1.5	600	0	233	370	3	18	267	102	267	369
2.2	1200	0	270	402	4	29	275	125	275	400
2.0	1200	0	482	747	9	68	505	232	505	737
1.5	1200	0	200	339	6	41	246	92	246	338
2.2	600	4	490	684	4	30	450	217	450	677
2.0	600	4	820	1160	8	58	786	359	786	1145
1.5	600	4	475	741	7	48	540	200	540	740
2.2	1200	4	415	610	6	45	420	186	420	606
2.0	1200	4	751	1121	12	87	785	322	785	1107
1.5	1200	4	365	627	11	78	626	163	626	626

A3 Results from mocks

With the comparisons of the two previous subsections, we have not been able to really quantify the difference between the proposed isolation criteria, even though our results hint towards the fact that the isolation criterion proposed by McKay et al. is probably the least appropriate of the three considered and that the one by Prada et al. seems to identify slightly more ‘large systems’ than ours. Therefore, in this section, we use the mocks and address the issue of the radial dependence of the satellite velocity dispersion, which Prada et al. found clear evidence for in their data.

In Fig. A3 we show a comparison between the different selection criteria used by McKay et al. (left panel), Prada et al. (central panel) and us (right panel). The aim is to show how well each of these different selection criteria succeed in recovering the ‘underlying’ satellite velocity dispersion, for which the median is given by the solid lines, and the dotted lines represent the 16th and 84th percentiles of the satellite velocity distribution as measured from the simulation cube. For comparison purposes, we have chosen to present in each panel the results within two different projected radii, as in Prada et al. (2003): $15 < r_p/h^{-1}$ kpc < 90 and $175 < r_p/h^{-1}$ kpc < 250 .

First of all we note that the different criteria are not all as successful in recovering the underlying satellite velocity dispersion. Clearly the one proposed by McKay et al. (i.e. left panel of Fig. A3) is the least successful, as it systematically gives an underestimate of the satellite velocity dispersion. This is especially true for the outer radial bin, for which the measured satellite velocity dispersion is barely within the 16th percentile of the underlying satellite velocity dispersion distribution. Moreover we note that for the mocks there are not enough faint primary systems for which this satellite criterion is satisfied, explaining why no velocity dispersion measurement is given for primaries fainter or equal to M^* . Interestingly, this is not true for the real data, for which there are still several faint primary satellite systems satisfying the isolation criterion. With larger number statis-

tics, this could be a potential way of constraining certain galaxy formation models, an approach followed up by van den Bosch et al. (2005).

The middle and right panels of Fig. A3 look more similar, in the sense that they both recover, within the errors, the ‘underlying’ satellite velocity dispersion, for both projected radial bins. However, three small differences can be noted. Firstly, the velocity dispersion errors around bright primaries are much larger using the isolation criterion of Prada et al. (2003). We note that the consistency between expectation and measurement is only reached due to large non-symmetrical errors. Secondly, the median satellite velocity dispersion in the outer projected radial bin is less accurately recovered with the isolation criterion of Prada et al. (2003). Indeed, both real and redshift space measurements have a tendency to predict a much flater luminosity-velocity dispersion relation than the underlying one. Thirdly, the real space measurements obtained with the isolation criterion of Prada et al. (2003) severely underestimate the true underlying velocity dispersion, especially for the brighter primaries.

Finally we note that, for our mock catalogue, there is virtually no radial dependence of the satellite velocity dispersion on the choice of radial shell (the distributions indicated by the bold and shaded lines are all in very good agreement with each other). It is worth pointing out that of the three proposed isolation criteria, only the one proposed by Prada et al. hints at a radial dependence of the satellite velocity dispersion. The trend is definitively weak and would be insignificant if the errors happen to be underestimated, or even just assumed to be symmetrical. The fact that this can happen is a potential worry for the claim made by Prada et al. (2003) for a radial dependence of the satellite velocity dispersion.

A4 Conclusions for SDSS comparison

We now have to address the question of whether our claim, that the isolation criteria of Prada et al. and McKay et al.

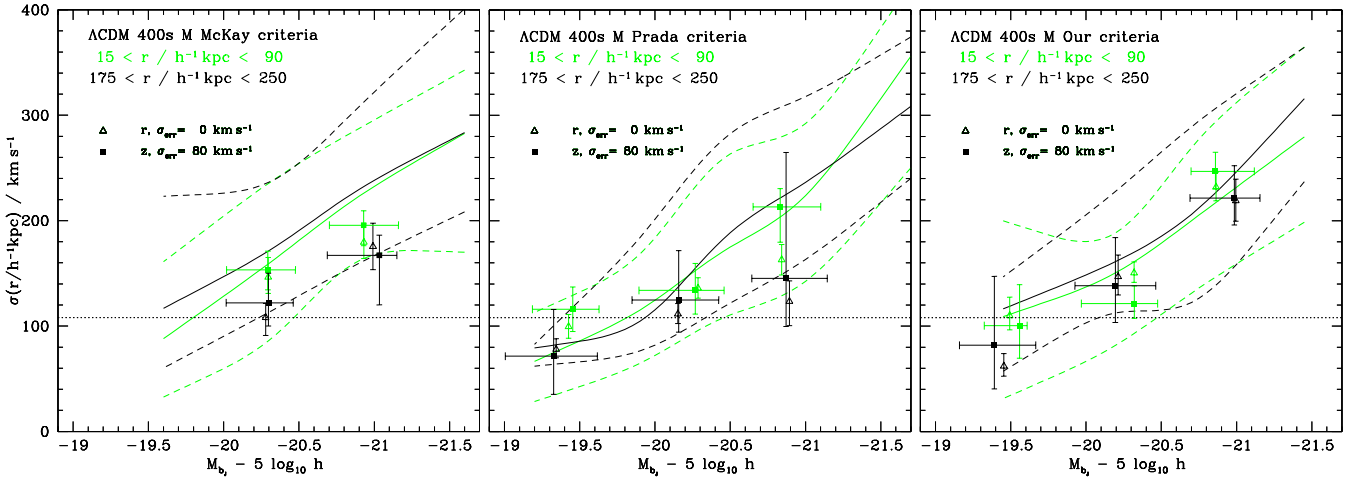


Figure A3. Mock results using the isolation criteria of McKay et al. (left panel), of Prada et al. (centre), and of this paper (right panel). The symbols with errorbars correspond to the real (open triangle) and redshift (filled square) space satellite velocity dispersion measurements around mock primaries identified using different selection criteria. The lines correspond to the median (solid) and 16th and 84th percentiles of the underlying primary satellite velocity dispersion. The different shadings correspond to two different cylindrical shells, whose ranges are given in the panel.

are more relaxed than our standard ones, is consistent with the differences found between the estimated velocity dispersions. Looking at the systematic difference between velocity dispersion measurements made with the two criteria, what we find is quite counter intuitive. One would probably expect, that relaxing the isolation criterion would result in measuring larger satellite velocity dispersions, whereas the opposite is found. This can probably related to a third difference between our nominal satellite selection criterion and the one used by Prada et al. : the length of the cylinder, within which satellite galaxies need to reside in order to be considered in the velocity dispersion estimate. Using Monte-Carlo realizations of satellite samples⁶ drawn from a ‘Gaussian plus a constant’ velocity distribution, we see that if one uses exactly the same velocity criterion as in Prada et al. (i.e. $\Delta V_s = 500$ km s $^{-1}$), one starts to systematically underestimate the velocity dispersion of systems with intrinsic velocity dispersion larger than 180 km s $^{-1}$. At the same time, one systematically overestimate the background for those systems. Taking into account the velocity errors, this translates, in the case of the 2dFGRS, to systems which are best fit by a velocity dispersion of around or larger than ~ 210 km s $^{-1}$, corresponding to all primaries slightly brighter than M^* (see e.g. Fig. 7). On those grounds, we motivate therefore the use of a deeper cylinder than Prada et al. in order to accurately measure the velocity dispersion of slightly larger systems. Our Monte-Carlo approach shows that we could have adopted a limiting velocity difference of 900 km s $^{-1}$ for spiral primaries, whereas there is a need, for elliptical primaries, to go out to ~ 1200 km s $^{-1}$, in order to appropriately sample the satellite velocity distribution.

⁶ i.e. with same number of systems as in the 2dFGRS, with similar distribution of satellites per system, and with the inclusion of an intrinsic maximal 10 to 20 % variation in the background and in the underlying velocity dispersion, so as to mimic to some extent that all systems are not exactly identical.

Therefore, most of the discrepancy between our analysis and the two using SDSS data reside in the different selection criteria used. From our results using the mock catalogues, from our Monte-Carlo simulations and from statistics of large systems discovered by the isolation criteria, there is a hint in the direction that the relaxed isolation criteria used by McKay et al. and Prada et al. are not as appropriate for finding dynamically isolated systems as our more stringent isolation criterion. Nevertheless we have to point out that the data is not yet good enough to be able to fully discriminate between the methods chosen.

Finally, a closer inspection of the two SDSS works shows that their findings are slightly different, something which was already pointed out in the analysis of Prada et al. (2003). Indeed the outer radii within which the velocity dispersions are measured are very different. As Prada et al. claim a strong dependence of the satellite velocity dispersion on radius, the agreement seen in Fig. 13 is not as good as it looks. On this last point, we would like to add, that we are not able, with our isolation criterion applied to the 2dFGRS, to detect such a signal. We know that the behaviour for ellipticals and spirals is rather different as function of luminosity, and therefore it could be legitimate to ask whether the effect seen by Prada et al. as function of projected radius could be due to a change in their sample mix as function of luminosity. Indeed with our findings, for galaxies of similar brightness, ellipticals will reside in much larger haloes than spirals. Hence stacking galaxies together irrespective of their morphological type, as done by Prada et al. (2003), could give rise to a velocity dispersion which depends on the radius within which it is measured. With our samples we are not able to reliably examine this issue, as it requires the samples to be split by morphological type, luminosity and projected radius. The only conclusion we can draw from our samples is that we observe a trend indicating that satellite velocity dispersion measurements of galaxies residing in the range $175 \leq r_p / h^{-1} \text{ kpc} \leq 375$ do not contain much infor-

mation. This is in perfect agreement with the fact that the measured satellite velocity dispersions within $375 h^{-1}$ kpc are identical, to within the errors, to those measured within $175 h^{-1}$ kpc.

APPENDIX B: COMPARISON WITH BRAINERD & SPECIAN AND BRAINERD

Regarding a comparison with the measurements of Brainerd & Specian (2003), for which in Fig. 13 ellipticals and spirals are shown by dashed-connected filled and open pentagons respectively, we first need to point out that they have used a similar selection criterion to the one proposed in Prada et al. (2003). For that reason, we expect, as explained above, to find differences between their results and our standard ones. However, like we did for Prada et al., we should be able to recover their results by assuming the same selection criterion.

For their sample of satellites around spiral primaries, it is impossible to recover their results for the following reasons. Firstly, they have forgotten to subtract the *rms* velocity measurement errors in quadrature, which in their case are of the same order of magnitude as ours, i.e. $\sim 110 \text{ km s}^{-1}$ (as they use data from the 2dFGRS 100k release). Secondly, in some way, the isolation criterion they have applied have to be wrong, as it is impossible to understand how they initially find an isolated system with more than 605 satellites. This is even larger than the largest galaxy cluster found in the complete 2dFGRS by Eke et al. (2004). In all likelihood they must have forgotten to deal with effects due to 2dFGRS 100k window function, which is extremely patchy, and hence very unsuitable for this type of study. Similarly, they have probably not used the full photometric input catalogue to reject systems which were not fully observed. For these reasons, their velocity dispersion measurements around spiral galaxies, from data which is a subsample of what we used in this analysis, are strongly erroneous.

Regarding their subsamples of elliptical primaries, there is no reason not to believe that they are affected by the same problems as their sample of spiral galaxies. However, due to the fact that the intrinsic velocity dispersion of those systems is much larger, forgetting to subtract in quadrature the velocity errors does not influence the results by more than 10 to 15% systematically. On the other hand, we believe, due to their problems with the isolation criterion, that the errors they quote on the satellite velocity dispersion around elliptical primaries is probably underestimated, and that the very strong trend with luminosity is too large.

Finally, we note that we have not, at all, been able to reproduce their results using either the full 2dFGRS sample nor the 2dFGRS 100k release sample. We suspect therefore some of the above mentioned problems to be the cause of these difference.

Recently, Brainerd (2005) made a new satellite analysis using the full 2dFGRS survey. Like for the Brainerd & Specian (2003) work, we are unable to reproduce in detail their findings, especially for faint primaries.

APPENDIX C: COMPARISON WITH VAN DEN BOSCH ET AL.

Finally, the results from van den Bosch et al. (2004), shown by dot-connected filled triangles in Fig. 13, clearly show that, with an isolation criterion that is too relaxed, the proposed method no longer finds a majority of dynamically isolated systems. Hence their criteria, as already discussed in their paper, were not intended and should not be used for selecting systems for dynamical studies.

We note that the analytic method presented in van den Bosch et al. (2004) for the luminosity - velocity dispersion relation, derived for their conditional luminosity function model, is in very good agreement with our measurements of that same relation from our semi-analytic mocks. Moreover, applying our isolation criteria to van den Bosch et al. (2004)'s conditional luminosity function mocks, we recover the underlying luminosity - velocity dispersion relation to great accuracy. This is a very strong consistency test for two completely different sets of models, constructed and constrained by different mechanisms.